Quaternary International 603 (2021) 40–63

Contents lists available at ScienceDirect

Quaternary International

journal homepage: www.elsevier.com/locate/quaint

Taxonomy, taphonomy and chronology of the Pleistocene faunal assemblage at Ngalau Gupin cave, Sumatra

Holly E. Smith [a,*], Gilbert J. Price [b], Mathieu Duval [c,a], Kira Westaway [d], Jahdi Zaim [e], Yan Rizal [e], Aswan [e], Mika Rizki Puspaningrum [e], Agus Trihascaryo [e], Mathew Stewart [f], Julien Louys [a]

[a] Australian Research Centre for Human Evolution, Environmental Futures Research Institute, Griffith University, Nathan, Queensland, 4111, Australia
[b] School of Earth and Environmental Sciences, The University of Queensland, St Lucia, Queensland, 4072, Australia
[c] Centro Nacional de Investigación Sobre la Evolución Humana (CENIEH), Burgos, 09002, Spain
[d] Department of Earth and Environmental Sciences, Macquarie University, Sydney, New South Wales, Australia
[e] Geology Study Program, Institut Teknologi Bandung, Jawa Barat, 40132, Indonesia
[f] Extreme Events Research Group, Max Planck Institutes for Chemical Ecology, the Science of Human History, and Biogeochemistry, Jena, Germany

ARTICLE INFO

Keywords:
Taxonomy
Taphonomy
Cave
Pleistocene
Southeast Asia
Hexaprotodon
ESR and U-series dating

ABSTRACT

Ngalau Gupin is a broad karstic cave system in the Padang Highlands of western Sumatra, Indonesia. Abundant fossils, consisting of mostly isolated teeth from small-to large-sized animals, were recovered from breccias cemented on the cave walls and unconsolidated sediments on the cave floor. Two loci on the walls and floors of Ngalau Gupin, named NG-A and NG-B respectively, are studied. We determine that NG-B most likely formed as a result of the erosion and redeposition of material from NG-A. The collection reveals a rich, diverse Pleistocene faunal assemblage (Proboscidea, Primates, Rodentia, Artiodactyla, Perissodactyla, Carnivora) largely analogous to extant fauna in the modern rainforests of Sumatra. The hippopotamid *Hexaprotodon* represents the only globally extinct taxon in deposits from Sumatra and the first record of this animal from the island. This fossil assemblage is dated using combined U-series/ESR dating analyses of several teeth that yield a finite age of between ~160 and ~115 ka, depending on the modalities of the dose rate evaluation. Moreover, a direct U-series age estimate of ~70 ka is obtained on the *Hexaprotodon* specimen, providing a minimum age constraint for the fossil that is compatible with the combined U-series/ESR results. These results suggest that the faunal assemblage at Ngalau Gupin correlates with late MIS 6 or early MIS 5. Ngalau Gupin likely reflects the formation of a fossil assemblage with two primary taphonomic pathways: a prime-aged dominated macrofauna component initially produced by carnivores but subsequently accumulated by porcupines and transported to the cave, and a microfauna component likely accumulated by small carnivores. Decalcification of the cemented deposit has further resulted in loss of fossil and other sedimentary material. This site adds important new chronologically constrained fossil mammal data for the Pleistocene record of Sumatra, an island relatively poorly investigated for Southeast Asia.

1. Introduction

The geological evolution and tropical climate of Southeast Asia created a global hotspot of biodiversity throughout the Pleistocene (Louys, 2008; Louys et al., 2007; Woodruff, 2010). Southeast Asia has a rich and interesting hominin history, highlighted by recent findings from Lida Ajer Cave, Sumatra, that demonstrate that *Homo sapiens* arrived in Southeast Asia before 63 ka - earlier than previously believed (Westaway et al., 2017); as well as other important hominin sites such as Trinil (Joorderns et al. 2009, 2015) and Ngandong, Java (Rizal et al., 2020) and Niah cave, Borneo (Barker et al., 2007). Many sites preserve a diverse suite of extant and extinct medium-to large-bodied mammals important for understanding the biogeographical and palaeoenvironmental history of the region (van den Bergh et al., 2001; Louys and Meijaard, 2010; Louys and Roberts, 2020). However, tropical caves are dynamic settings with complex formational processes, meaning it

* Corresponding author.
E-mail address: holly.smith11@griffithuni.edu.au (H.E. Smith).

https://doi.org/10.1016/j.quaint.2021.05.005
Received 28 May 2020; Received in revised form 5 May 2021; Accepted 6 May 2021
Available online 15 May 2021

can be incredibly difficult to discern the taphonomic history of palaeontological and early human remains found within them (O'Connor et al., 2010; Morley and Goldberg, 2017; Smith et al., 2020). Studying mechanisms of site formation, depositional history, and faunal accumulation in Southeast Asian caves is therefore critical to our understanding of animal and hominin prehistory in Pleistocene Southeast Asia. Yet, compared to other regions such as tropical Africa, much less attention has been devoted to understanding the taphonomic and depositional histories of assemblages in tropical Southeast Asia.

During the last couple of decades, research has increasingly focussed on the faunal assemblages in the caves of Southeast Asia as a basis to resolve stratigraphic and depositional complexities (e.g. Bacon et al., 2004; Barker et al., 2007; Westaway et al., 2007; O'Connor et al., 2010; Mijares et al., 2010; Duringer et al., 2012; Bacon et al., 2015; Stephens et al., 2017; Morley et al., 2017; Louys et al., 2017; Westaway et al., 2017; Zeitoun et al., 2019). Nevertheless, few studies have been undertaken in the region of the Padang Highlands, the area with the earliest dated records of humans in the region (Westaway et al., 2017). Much of what we know about the Sumatran fossil record comes from palaeoanthropologist Eugene Dubois, (1891) and palaeontologist Dirk Albert Hooijer (Hooijer 1947a, 1947b, 1948, 1960, 1947b), who reported on and studied fossils from numerous caves, including Lida Ajer, Sibrambang, and Djamboe. Contextual information regarding these sites is largely missing, however, as many of the excavations were carried out prior to the development of modern excavation methods and, with the exception of Lida Ajer, because Dubois did not keep detailed field notes. The discovery in 2015 of a new fossil assemblage at Ngalau Gupin cave in the Padang Highlands (Louys et al., 2017) provides us with a unique opportunity to examine the taphonomic pathways fossils can take in a tropical cave setting. Here, we report on the taxonomy, taphonomy, and chronology of the vertebrate fossils from Ngalau Gupin.

2. Ngalau Gupin

Ngalau Gupin is a large limestone cave complex approximately 90 km east of Sawah Lunto City (00′ 38.685 S, 100' 38.823 E) (Fig. 1). This cave formed as part of a comprehensive karst system in Carboniferous-Permian limestones that includes several other previously reported caves (Dubois, 1891; Louys et al., 2017). Ngalau Gupin was first reported by Louys et al. (2017) as part of a survey of island Southeast Asian caves. Spot collection of isolated teeth from the Ngalau Gupin deposits was carried out, and initial U–Th dating of a *Tapirus* molar produced a preliminary minimum age of ~45 ka (Louys et al., 2017).

2.1. Site description

The site is easily accessed due to a relatively horizontal entrance and flat floor, walls and high ceiling. The entrance opens into a wide corridor that extends 15 m west and sits within the photic zone of the cave. The corridor opens almost immediately into a large cavernous chamber, averaging 12 m in width and 5 m in height. Abundant well-preserved Pleistocene fossiliferous breccia and sediments were identified in and around a phreatic U-shaped passage raised approximately 5 m from the lower cave floor (Fig. 2).

Breccia is present in two discrete areas in the U-shaped passageway. Non-fossiliferous breccia is visible on the eastern wall, evident as a 0.3 m deposit that hangs at most 2 m from the cave floor. The fossil-bearing breccia Ngalau Gupin-A (NG-A) is identifiable along the westernmost wall reaching a height of up to 1 m above the cave floor (Fig. 3). The breccia of NG-A represents a dense, lightly cemented mosaic deposit of angular clasts from pebble to cobble size within a clay-rich matrix. It is quite crumbly and appears significantly decalcified. Fossils were in general easily removed from this breccia by hand and pick.

Ngalau Gupin-B (NG-B) is demarcated as the unconsolidated fossil-bearing sediments visible on the topmost layer of the floor directly north of the U-shaped passageway (Fig. 4). NG-B has a surface area of approximately 5 × 5 m and a depth of ~10 cm, and visibly erodes to muddy topsoil that slopes approximately 2 m across the cave floor. The sediment deposits containing the NG-B assemblage are an unconsolidated clay-rich mud matrix.

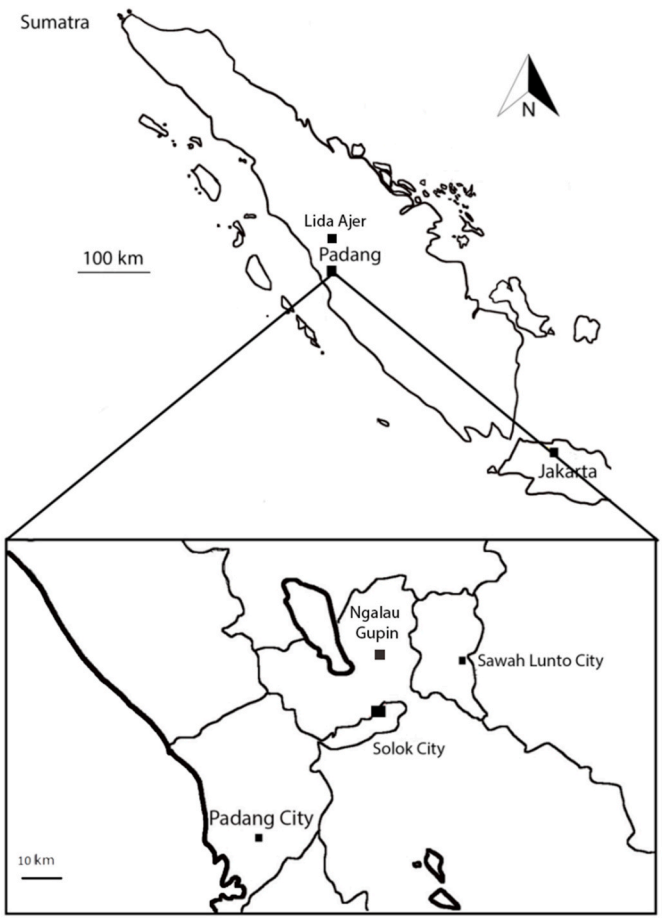

Fig. 1. Map of Sumatra illustrating the location of Padang (inset) and western Sumatra illustrating the location of Ngalau Gupin.

3. Methodology

3.1. Survey and excavation

In order to map the cave system, we performed a cave line survey, mapped by noting the orientation and inclination of the individual rooms and passages of Ngalau Gupin. These measurements were taken and recorded at regular intervals along a line transect and the two-dimensional data was used to form a scaled geometrical representation of the cave in lateral and plan view. Fossils visible in the breccia deposits were excavated using hammers and chisels. To remove adhering matrix, fossils were soaked in water for 24 h before mechanical preparation with a dental drill. The NG-B fossils in the unconsolidated sediments were excavated using trowels to a depth of 10 cm across a surface area of 3 × 1 m, with one protruding section in the west extending a further 1 × 0.5 m. The sediment was sieved through a 5 mm mesh and all faunal material was collected.

3.2. Systematic palaeontology

Every fossil specimen was identified to the lowest possible taxonomic level. The dimensions of the specimens were compared to osteological collections housed at the Oxford Museum of Natural History, the Natural History Museum of London, Lee Kong Chian Natural History Museum,

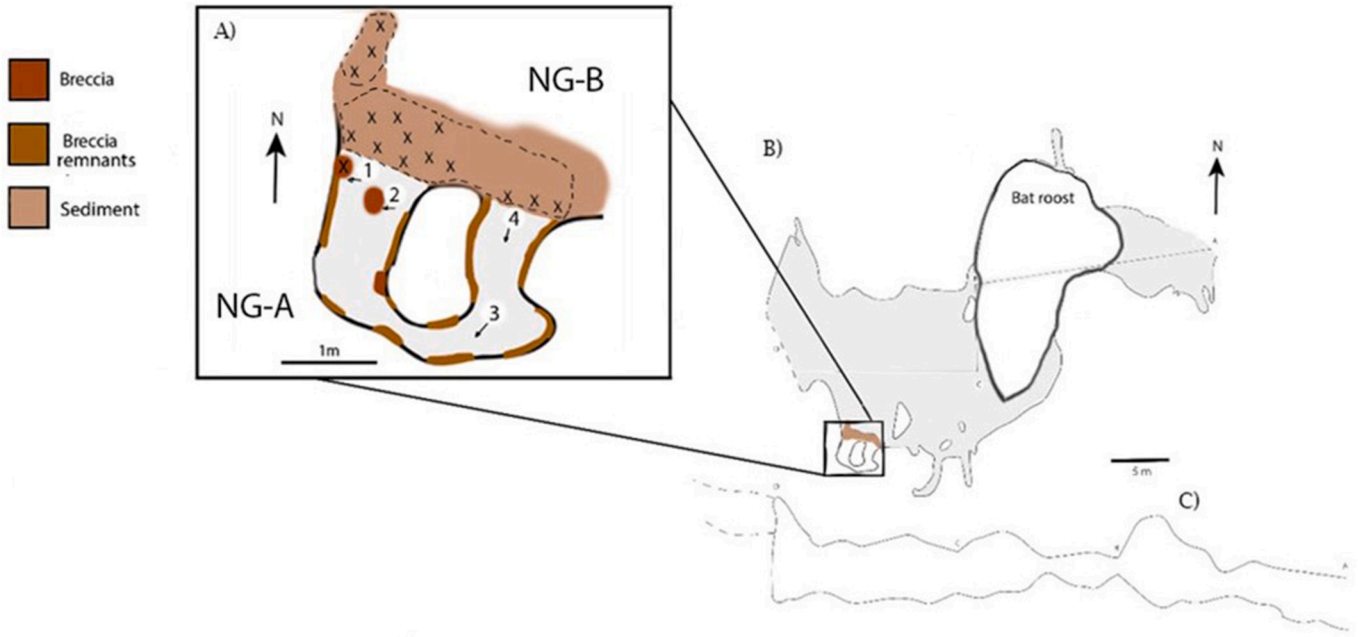

Fig. 2. Ngalau Gupin fossil site. A) Plan view of Ngalau Gupin breccia sites (inset); 1–4 are photograph locations and orientations presented in Fig. 3, the two areas indicated with the dashed lines are the sites of fossil excavation; the X indicates the presence of fossils in NG-B; B) plan view scale cave survey of Ngalau Gupin; C) lateral view scale cave survey of Ngalau Gupin.

American Museum of Natural History and Zoologische Straatssammlung München. Classic measurements on teeth were taken to the nearest 0.1 mm. Dental nomenclature for each taxon was taken from well-established literature: Dental nomenclature for each taxon was taken from well-established literature: proboscideans (Maglio, 1927); felids (Hillson, 2005); viverrids (Popowics, 2003); *Helarctos* (Raffles, 1821 and Fitzgerald and Kraussman, 2002); primates (Kay, 1975; Teaford, 1982; Hooijer, 1948, 1960 and Drawhorn, 1995); *Hystrix* (Van Weers, 1990, 1993, 2005); rhinocerotids (Yan et al., 2014); suids (Cucchi, 2009); bovids (Hooijer, 1958; Suraprasit et al. 2016, 2020); cervids (Leslie, 2011; Chapman et al., 2005; Suraprasit et al., 2016); tragulids (Mennecart, 2018).

3.3. Taphonomic analysis

Taphonomic analysis was carried out following the established methods described below with each specimen examined by eye and hand lens (10x). Quantitative results are presented as Number of Identified Specimens (NISP) and the Minimum Number of Individuals (MNI) (Chaplin, 1971; Badgley, 1986; Lyman, 2008). MNI was calculated using the most abundant skeletal element or tooth and taking into consideration side (left/right) for bilaterally paired elements and age of the individual (Bunn et al., 1986). Elements were placed into an animal size class adapted from Bunn (1982); category I-II (<1 kg), category III-IV (1–10 kg), category V-VI (10–100 kg), category VII-VIII (100–340 kg) and category VIII-IX (>340 kg). Each specimen was assigned a weathering stage ranging from zero to five (following Behrensmeyer, 1978). Abrasion was recorded as: (1) little or no abrasion, retaining fresh, sharp edges; (2) moderate abrasion, exhibiting some rounding to breaks; and (3) heavy abrasion, with well rounded edges (following Shipman, 1977). Long bone fracture angle (oblique, right, oblique/right), outline (curved, transverse, intermediate), and edge (smooth, jagged) was recorded following Villa and Mahieu (1991). The animal age class was categorised by recording the wear stage of all whole teeth in the record in four categories: stage one, no apparent wear; stage two, little shear apparent and cusps blunted on most teeth; stage three, moderate shear apparent on facets and cusps; and stage four, strong shear facets and/or blunted cusps, premolars and molars very well-rounded. This categorisation was adapted from Brown and Chapman (1991) for Cervidae, Fitzgerald & Kraussman (2002) for Ursidae, Rolett and Chiu (1994) for Suidae, Hillson (2005) for Felidae, Tong et al. (2002) for Rhinocerotidae, Maffei (2003) for Tapiridae, Bowen and Coch (1970), Kay and Cant (1988), Bunn and Ungar (2009) for Cercopithecidae, Van Aarde (1985) for Hystricidae, and Sten (2004) for Bovidae. We used wear criteria given by crown height measurements in each of the relevant literatures to determine age classes for each taxon. Statistical analyses were carried out using PAST ver. 2.17c (Hammer et al., 2001). We list only representative specimens of each taxon evident in the collection (c.f. Leroy and Levinson, 1974; Hilton et al., 2001; Baludikay et al., 2016; Florin et al., 2020). The full taphonomic catalogue is available on an element-by-element database in the supplementary information (Table S10). The measurements in the database correspond to the anatomical tooth measurements described in section 3.2.

3.4. Abbreviations

Field numbers are denoted by the code SUMXX-xx, where XX refers to the year of collection and xx refers to the field number. From fieldwork undertaken in 2015, the NG-A specimens are identified with the abbreviation ‘GUP1-51’ and NG-B specimens are identified with abbreviation ‘GUP52-81’. From fieldwork undertaken in 2018, the NG-A specimens are identified with the abbreviations ‘GG’, and NG-B specimens identified with the abbreviation ‘NG’. Isolated specimens found within the cave but outside the NG-A and NG-B boundaries are denoted with ‘GU’. All specimens are stored at Paleontologi dan Geologi Kuarter, Institut Teknologi Bandung, Indonesia.

3.5. Uranium profiling and combined U-series/ESR dating

3.5.1. Material

Six fossil teeth were collected from the cemented breccia and unconsolidated sediment deposits from Ngalau Gupin (Supplementary information Table S2) for uranium concentration profiling and/or direct dating, three from NG-A (SUM18-21, SUM18-26 & SUM18-27) and three from NG-B (SUM18-22, SUM18-24 & GG4.1). Among these fossil teeth, five of them were dated using the combined U-series/ESR dating

method, while the *Hexaprotodon* specimen GG4.1 was dated with U-series only. Corresponding sediment samples were collected at each locus (NG-A: SUM18-11; NG-B: SUM18-12) for dose rate reconstruction. The breccia matrix from NG-A was sampled for post infrared-infrared stimulated luminescence (pIR-IRSL) dating. This sample yielded very few potassium feldspar grains in the datable size range (90–212 μm) as seen in the Lida Ajer breccia (Westaway et al., 2017) and Ngalau Sampit (Duval et al. *in prep*). This amounted to only one single-grain disc of <100 grains, but none of these grains produced a measurable IRSL decay thereby preventing a reliable age estimation to be obtained.

3.5.2. Sample preparation

The five teeth were prepared following the standard ESR dating procedure based on enamel powder: the enamel layer was mechanically separated from the other dental tissues and both inner and outer surfaces were removed with a dentist drill to eliminate the volume that received an external alpha dose. The dentine attached to the enamel layer was kept aside for subsequent solution bulk U-series analyses. Enamel and dentine were ground and sieved <200 μm. Unlike the other teeth dated, SUM18-21 was collected embedded in a breccia. The tooth was therefore extracted from the sediment, which was subsequently sampled for

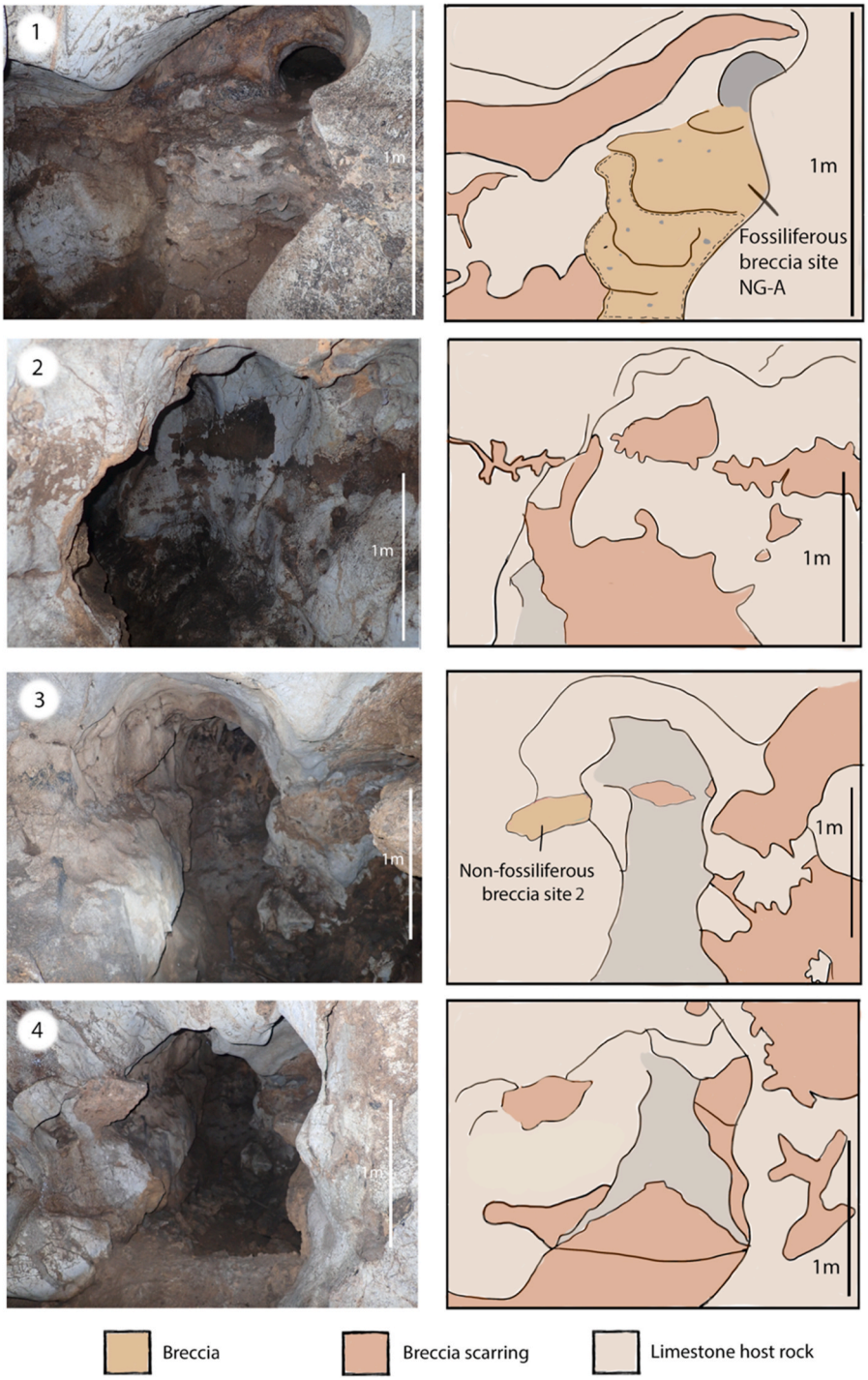

Fig. 3. Specific breccia remains observed in Ngalau Gupin at the excavation site of the NG-A assemblage. A-D) for locations and orientations of photographs refer to Fig. 2; (right) corresponding annotated sketches of photographs of breccia bearing site in Ngalau Gupin. The area within the dashed lines indicate the area that fossils were excavated from NG-A.

further analysis.

For uranium concentration profiling and U-series dating of sample GG4.1, powders were drilled across a transect from the enamel through the dentine using a 1 mm diameter stainless steel bit (see Price et al., 2013 for additional methodological details). GG4.1 was not further sampled for more destructive ESR dating considering its fragility and rarity as a representative specimen of *Hexaprotodon* in the deposit.

3.5.3. ESR dose evaluation

Dose evaluation used the multiple aliquot additive dose (MAAD) method. The enamel powder of sample SUM1821 was split into ten aliquots and gamma-irradiated at CENIEH (Spain) with a Gammacell 1000 Cs-137 gamma source (dose rate = 6.39 ± 0.15 Gy/min) to the following doses: 0.0, 49.9, 99.8, 149.6, 249.5, 349.2, 498.9, 698.5, 898.1 and 1496.8 Gy. The other enamel samples were irradiated at ANSTO (Australia) with a Co-60 source (dose rate = 13.23 ± 0.21 Gy/min) as follows: 0.0, 42.5, 83.3, 127.5, 206.8, 295.2, 427.7, 589.2, 769.0, 1283.0 and 2966.0 Gy.

Room temperature ESR measurements were carried out at CENIEH with an EMXmicro 6/1 Bruker ESR spectrometer coupled to a standard rectangular ER 4102ST cavity. The following procedure was used to minimise the analytical uncertainties: (i) all aliquots of a given sample were carefully weighted into their corresponding tubes and a variation of <1 mg was tolerated between aliquots; (ii) ESR measurements were performed using a Teflon sample tube holder inserted from the bottom of the cavity to ensure that the vertical position of the tubes remains exactly the same for all aliquots. The following acquisition parameters were used: 1–50 scans, 1 mW microwave power, 1024 points resolution, 15 mT sweep width, 100 kHz modulation frequency, 0.1 mT modulation amplitude, 20 ms conversion time and 5 ms time constant. All aliquots of

Fig. 4. Fossiliferous sediments of NG-B and the entrance to the east and west passageways containing the NG-A remains excavated from consolidated breccia; (below) annotated sketch of the fossiliferous sediments containing the NG-B assemblage. The area within the dashed lines indicate the area in which the NG-B fossils were excavated.

a given sample were measured within a short time interval (<1 h). This procedure was repeated two to three times over successive days without removing the enamel from the ESR tubes between measurements in order to evaluate measurement and equivalent dose (D_E) precisions (Supplementary Information Table S3).

The ESR intensities were extracted from T1-B2 peak-to-peak amplitudes of the ESR signal (Grün, 2000a), and then normalized to the corresponding number of scans and aliquot mass. D_E values were obtained by fitting a single saturating exponential (SSE) through the mean ESR intensities derived from the repeated measurements. Fitting was performed with Microcal OriginPro 9.1 software, which is based on a Levenberg-Marquardt algorithm by chi-square minimisation. Data were weighted by the inverse of the squared ESR intensity ($1/I^2$) (Grün and Brumby, 1994). ESR dose-response curves (DRCs) are shown in Supplementary Figure S1. Final 1-σ D_E error used for age calculation include both the fitting and gamma source dose rate errors.

3.5.4. Solution U-series analyses of dental tissues

Powdered enamel and dentine samples were weighed then spiked using a 229Th-^{233}U tracer before being digested in concentrated HNO_3. The solutions were then treated with H_2O_2 to remove trace organics, with U and Th then separated using conventional column chemistry techniques described in Clark et al. (2014). Both U and Th were collected into the same pre-cleaned test tube using 3 ml of 2% HNO_3 mixed with a trace amount of HF. U–Th isotopic ratios were then measured using a Nu Plasma multi-collector inductively-coupled plasma mass spectrometer (MC-ICP-MS) in the Radiogenic Isotope Facility at The University of Queensland, Brisbane, Australia, following analytical protocols described in Zhao et al. (2009), Price et al. (2013), and Clark et al. (2014).

3.5.5. Dose rate evaluation and age calculations

No *in situ* evaluation of the gamma dose rate associated with the teeth was performed. For all teeth except SUM18-21, both the beta and gamma dose rates were derived from the laboratory analysis of the corresponding bulk sediment samples collected at each locus. In contrast, for SUM18-21, two scenarios were considered, with beta and gamma dose rate derived from either the breccia sediment collected from around the tooth (a) or from sediment sample SUM18-11 collected at NG-A (b).

Inductively Coupled Plasma Mass Spectrometry (ICP-MS) analyses were performed on all sediment samples by Genalysis Laboratory Services, following a four-acid digest preparation procedure. The following parameters were used for the dose rate calculations: an alpha efficiency of 0.13 ± 0.02 (Grün and Katzenberger-Apel, 1994), Monte-Carlo beta attenuation factors from Marsh (1999), dose-rate conversion factors from Guérin et al. (2011), an assumed water content 5 ± 3 wt% in dentine. Current water (% wet weight) content in sediment samples SUM18-11 and SUM18-12 was evaluated to 24.9 and 26.6%, respectively. Consequently, a value of 25 ± 5% was assumed as long-term water content for all samples. Given the long distance between the cave entrance and the fossil teeth (>30 m), and the significant thickness of the overburden (ca. 30 m), the cosmic dose rate was assumed to be negligible. Post-Rn equilibrium was assumed in dental tissues and sediment.

DATA (Grün, 2009), a Quick Basic-based program was used to calculate US-ESR (based on the US model defined by Grün et al., 1988) and CSUS-ESR age estimates. The CSUS model defined by Grün (2000b) assumes a closed system behaviour after a rapid uranium uptake event in dental tissues. The CSUS-ESR age is usually considered as providing a maximum age constraint for the fossil. US and CSUS models are typically considered to encompass all possible uptake scenarios. Early uptake (EU)-ESR ages were also calculated for comparison. Finally, the accelerating uptake (AU) model (Shao et al., 2012) that can take into account uranium leaching was also tested. AU-ESR ages were obtained from USESR, a Matlab-based program (Shao et al., 2014). All combined U-series/ESR data inputs and outputs are given in Table 1.

4. Results

4.1. Taxonomic identifications

Class: Gastropoda Cuvier, 1795
Order: Stylommatophora Swainson, 1840
Representative specimen: GUP1 – mollusc – NG-A assemblage

(See Fig. 5, Fig. 5A)

GUP1 is a large mollusc. The spire, body whorl, and umbilicus of the shell are present, but the outer lip, palatal wall and columellar wall have been destroyed. The shell is depressed with five evident whorls; the apex of the shell has no growth lines and each whorl of the shell significantly increases in size from the interior to exterior. This sample has right-handed coiling. There are no identifiable ridges or plications to determine the genus of this specimen.

Order: Sigmurethra Bouchet & Rocroi, 2005
Family: Clausiliidae Gray, 1855
Representative Specimen: GUP27 – mollusc – NG-A assemblage

(Fig. 5B)

GUP27 is identifiable as a small brown Clausiliidae shell due to the oblong and elongate structure with five turreted whorls of equal size that coil sinistrally to a high spire (Loosjes, 1953; Dharma, 1992, 2005, 2005; Dharma et al., 2009). Shells are tapered at both ends and the aperture has a relatively oval shape and pronounced fold.

Class: Reptilia Laurenti, 1768
Order: Squamata Oppel, 1811
Family: Varanidae Merrem, 1820
Representative Specimens: NG4.1 – unidentified tooth – NG-B assemblage

(Fig. 5C)

This element is a sharp, pointed recurved tooth with a very lightly serrated edge. The tooth is laterally compressed and has two light ridges running down the lateral side of the tooth. This ridge is visible in the cross section of the tooth such that it is not perfectly circular. This dental morphology is typical of varanids (King and Green, 1999). There is a shallow depression in the tooth that extends across the enamel surface from either termination of the ridge. Overlapping morphology means that this tooth cannot be assigned to a species, however, varanids currently found in Sumatra include *Varanus dumerilii*, *Varanus rudicollis*, and *Varanus salvator*.

Class: Aves Linnaeus, 1758
Representative Specimens: NG34.17 – coracoid fragment - NG-B assemblage

(Fig. 5D)

NG34.17 is a coracoid with a transverse fracture along the shaft. The acrocoracoid process is present but poorly preserved. The general characteristics of the bone are typical of bird anatomy, such as the flaring out of the post coracoid process (Post, 2005; Kaiser, 2010), that is only partly preserved in this specimen. The lack of diagnostic material means that more specific identification is impossible.

Class: Mammalia Linnaeus, 1758
Order: Proboscidea Illiger, 1811
Family: Elephantidae Gray, 1821
Genus: *Elephas* Linnaeus, 1758
Elephas sp.
Representative specimen: GUP52 – molar fragment – NG-A assemblage

(Fig. 5F)

Table 1
Data inputs and outputs associated to the ESR age calculations. All errors are given at a 1σ confidence level. Key: (1) Apparent U-series ages are corrected for detrital Th. (2) A 10% error was assumed; (3) from sediment attached to SUM18-21; (4) from sediment sample SUM18-11 collected at NG-A; (5) from sediment sample SUM18-12 collected at NG-B; (6) corresponds to about 88% of the infinite-matrix gamma dose rate. In italics, AU-ESR age calculation outputs. SUM18-22a and SUM18-24a: age calculations using infinite matrix gamma dose rate; SUM18-22b and SUM18-24b: age calculations using 88% infinite matrix gamma dose rate.

SAMPLE	SUM18-21a	SUM18-21b	SUM18-22a	SUM18-22b	SUM18-24a	SUM18-24b	SUM18-26a	SUM18-26b	SUM18-27a	SUM18-27b
Locus	NG-A	NG-A	NG-B	NG-B	NG-B	NG-B	NG-A	NG-A	NG-A	NG-A
Enamel										
Dose (Gy)	35.1 ± 2.1	35.1 ± 2.1	32.8 ± 2.3	32.8 ± 2.3	33.6 ± 1.2	33.6 ± 1.2	26.1 ± 0.8	26.1 ± 0.8	22.2 ± 1.7	22.2 ± 1.7
U (ppm)	0.11 ± 0.00	0.11 ± 0.00	0.04 ± 0.00	0.04 ± 0.00	0.07 ± 0.00	0.07 ± 0.00	0.04 ± 0.00	0.04 ± 0.00	0.07 ± 0.00	0.07 ± 0.00
234U/238U	1.178 ± 0.004	1.178 ± 0.004	1.173 ± 0.003	1.173 ± 0.003	1.220 ± 0.006	1.220 ± 0.006	1.246 ± 0.003	1.246 ± 0.003	1.328 ± 0.006	1.328 ± 0.006
230Th/234U	0.390 ± 0.003	0.390 ± 0.003	1.438 ± 0.004	1.438 ± 0.004	0.582 ± 0.007	0.582 ± 0.007	0.397 ± 0.003	0.397 ± 0.003	0.430 ± 0.005	0.430 ± 0.005
230Th/232Th	34.8 ± 0.2	34.8 ± 0.2	38.7 ± 0.3	38.7 ± 0.3	64.8 ± 0.6	64.8 ± 0.6	34.7 ± 0.3	34.7 ± 0.3	79.9 ± 0.8	79.9 ± 0.8
Apparent U-series age (ka) (1)	52.1 ± 0.3	52.1 ± 0.3	60.8 ± 0.8	60.8 ± 0.8	91.1 ± 0.3	91.1 ± 0.3	53.2 ± 0.5	53.2 ± 0.5	59.3 ± 0.4	59.3 ± 0.4
Initial 234U/238U	1.209	1.209	1.208	1.208	1.287	1.287	1.289	1.289	1.390	1.390
Alpha Efficiency (1)	0.13 ± 0.02	0.13 ± 0.02	0.13 ± 0.02	0.13 ± 0.02	0.13 ± 0.02	0.13 ± 0.02	0.13 ± 0.02	0.13 ± 0.02	0.13 ± 0.02	0.13 ± 0.02
Water content (%)	0	0	0	0	0	0	0	0	0	0
Initial enamel thickness (μm) (2)	722 ± 72	722 ± 72	1803 ± 180	1803 ± 180	1474 ± 147	1474 ± 147	2467 ± 247	2467 ± 247	1593 ± 159	1593 ± 159
Dentine										
U (ppm)	5.28 ± 0.00	5.28 ± 0.00	4.47 ± 0.00	4.47 ± 0.00	3.37 ± 0.00	3.37 ± 0.00	4.66 ± 0.00	4.66 ± 0.00	3.70 ± 0.00	3.70 ± 0.00
234U/238U	1.148 ± 0.000	1.148 ± 0.000	1.062 ± 0.000	1.062 ± 0.000	1.052 ± 0.000	1.052 ± 0.000	1.097 ± 0.001	1.097 ± 0.001	1.091 ± 0.001	1.091 ± 0.001
230Th/234U	0.232 ± 0.001	0.232 ± 0.001	0.363 ± 0.001	0.363 ± 0.001	0.341 ± 0.001	0.341 ± 0.001	0.320 ± 0.001	0.320 ± 0.001	0.241 ± 0.000	0.241 ± 0.000
230Th/232Th	439.8 ± 1.7	439.8 ± 1.7	17950 ± 74	17950 ± 74	562.8 ± 1.7	562.8 ± 1.7	5972.0 ± 26.6	5972.0 ± 26.6	91.3 ± 0.2	91.3 ± 0.2
Apparent U-series age (ka) (1)	28.6 ± 0.1	28.6 ± 0.1	48.9 ± 0.1	48.9 ± 0.1	45.3 ± 0.1	45.3 ± 0.1	41.9 ± 0.0	41.9 ± 0.0	29.7 ± 0.1	29.7 ± 0.1
Initial 234U/238U	1.160	1.160	1.071	1.071	1.059	1.059	1.110	1.110	1.099	1.099
Water (%)	5 ± 3	5 ± 3	5 ± 3	5 ± 3	5 ± 3	5 ± 3	5 ± 3	5 ± 3	5 ± 3	5 ± 3
Removed enamel thickness (μm) (2)	7 ± 1	7 ± 1	239 ± 24	239 ± 24	115 ± 11	115 ± 11	212 ± 21	212 ± 21	211 ± 21	211 ± 21
Sediment										
U (ppm)	0.590 ± 0.072 (3)	3.720 ± 0.148 (4)	2.120 ± 0.101 (5)	2.120 ± 0.101 (5)	2.120 ± 0.101 (5)	2.120 ± 0.101 (5)	3.720 ± 0.148 (4)	0.590 ± 0.072 (3)	3.720 ± 0.148 (4)	0.590 ± 0.072 (3)
Th (ppm)	1.370 ± 0.075 (3)	3.040 ± 0.136 (4)	6.190 ± 0.263 (5)	6.190 ± 0.263 (5)	6.190 ± 0.263 (5)	6.190 ± 0.263 (5)	3.040 ± 0.136 (4)	1.370 ± 0.075 (3)	3.040 ± 0.136 (4)	1.370 ± 0.075 (3)
K (%)	0.441 ± 0.017 (3)	0.286 ± 0.011 (4)	0.434 ± 0.017 (5)	0.434 ± 0.017 (5)	0.434 ± 0.017 (5)	0.434 ± 0.017 (5)	0.286 ± 0.011 (4)	0.441 ± 0.017 (3)	0.286 ± 0.011 (4)	0.441 ± 0.017 (3)
Water (%)	25 ± 5	25 ± 5	25 ± 5	25 ± 5	25 ± 5	25 ± 5	25 ± 5	25 ± 5	25 ± 5	25 ± 5
Removed thickness (μm) (2)	34 ± 3	34 ± 3	15 ± 2	15 ± 2	110 ± 11	110 ± 11	77 ± 8	77 ± 8	18 ± 2	18 ± 2
US/AU-ESR age calculations										
internal dose rate (μGy/a)	11 ± 1	20 ± 4	*12 ± 12*	8 ± 1	*20 ± 1*	*19 ± 1*	*14 ± 1*	5 ± 1	*28 ± 1*	12 ± 2
beta dose rate, dentine (μGy/a)	23 ± 1	25 ± 2	*18 ± 18*	13 ± 2	*15 ± 1*	*13 ± 1*	*12 ± 1*	5 ± 0	*16 ± 1*	9 ± 1
beta dose rate, sediment (μGy/a)	54 ± 6 (3)	100 ± 11 (4)	*52 ± 4 (5)*	50 ± 6 (5)	*47 ± 4 (5)*	*46 ± 4 (5)*	*34 ± 4 (4)*	16 ± 2 (3)	*62 ± 6 (4)*	31 ± 4 (3)
Gamma + cosmic dose rate (μGy/a)	173 ± 14 (3)	460 ± 35 (4)	*465 ± 25 (5)*	409 ± 31 (5,6)	*465 ± 25 (5)*	*409 ± 31 (5,6)*	*460 ± 35 (4)*	173 ± 14 (3)	*460 ± 35 (4)*	173 ± 14 (3)
Total dose rate (μGy/a)	261 ± 15	606 ± 37	*547 ± 99*	481 ± 31	*547 ± 24*	*487 ± 31*	*520 ± 27*	200 ± 14	*555 ± 28*	225 ± 14
p enamel or *n enamel*	0.25	−0.93	*−0.025*	−0.92	*−0.027*	*−0.028*	*−0.030*	0.16	*−0.043*	−0.47
p dentine or *n dentine*	1.15	0.00	*−0.022*	−0.66	*−0.019*	*−0.015*	*−0.026*	.82	*−0.031*	−0.10
US-ESR age (ka) or *AU-ESR age (ka)*	**134 + 12–11**	**57 + 5–4**	***60 ± 10***	**68 + 7–6**	***61 ± 2***	***69 ± 3***	***50 ± 2***	**130 + 11–10**	***39 ± 3***	**98 + 10–9**
EU-ESR (ka)	**102 ± 7**	**53 ± 4**	**60 ± 5**	**67 ± 6**	**61 ± 4**	**68 ± 4**	**50 ± 3**	**119 ± 7**	**40 ± 4**	**90 ± 8**
CSUS-ESR (ka)	**141 ± 13**	**57 ± 5**	**60 ± 6**	**68 ± 7**	**60 ± 4**	**68 ± 5**	**50 ± 4**	**131 ± 10**	**39 ± 4**	**101 ± 10**

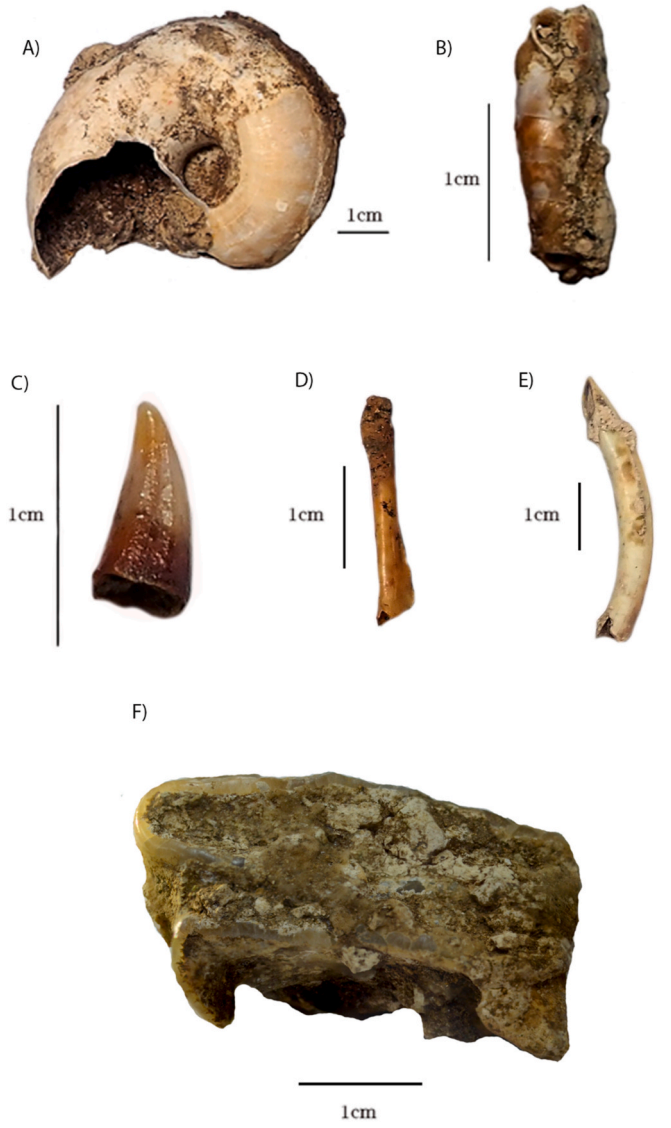

Fig. 5. (A) GUP1 Gastropoda shell in posterior view; (B) GUP27 Clausiliidae shell in posterior view; (C) NG4.1 Varanidae tooth; (D) NG34.17 Aves coracoid fragment; (E) NG3.38 *Hystrix* incisor in buccal view; (F) GUP52 *Elephas* sp. tooth plate fragment in occlusal view.

GUP52 is a molar fragment with typical hypsolophodont form. It preserves two elevated ridged enamel lamellae connected by depressed cementum. The enamel folds are heavily wrinkled and heavily worn. The widths of the lamellae (5.3 cm and 5.25 cm) are a strong indication that this fragment is an anterior section of a deciduous molar from a juvenile (Maglio, 1973). This specimen can be confidently assigned to Elephantidae as the two transverse cusp rows of the molar are fused into elevated loops of enamel with cementum infilling rather than roofed ridges (Zhang et al., 2017). It most likely belongs to *Elephas* sp.

Order: Primates, Linnaeus 1758
Family: Hominidae Gray, 1825
Genus: *Pongo* Lacépède, 1799
Pongo sp.
Representative Specimen: NG11.20 – left P^3 – NG-B assemblage

(See Fig. 6, Fig. 6A)

The premolar is bunodont with numerous prominent crenulations extending between a large, pointed paracone, and a slightly smaller protocone. These are divided by a deep anteroposterior valley.

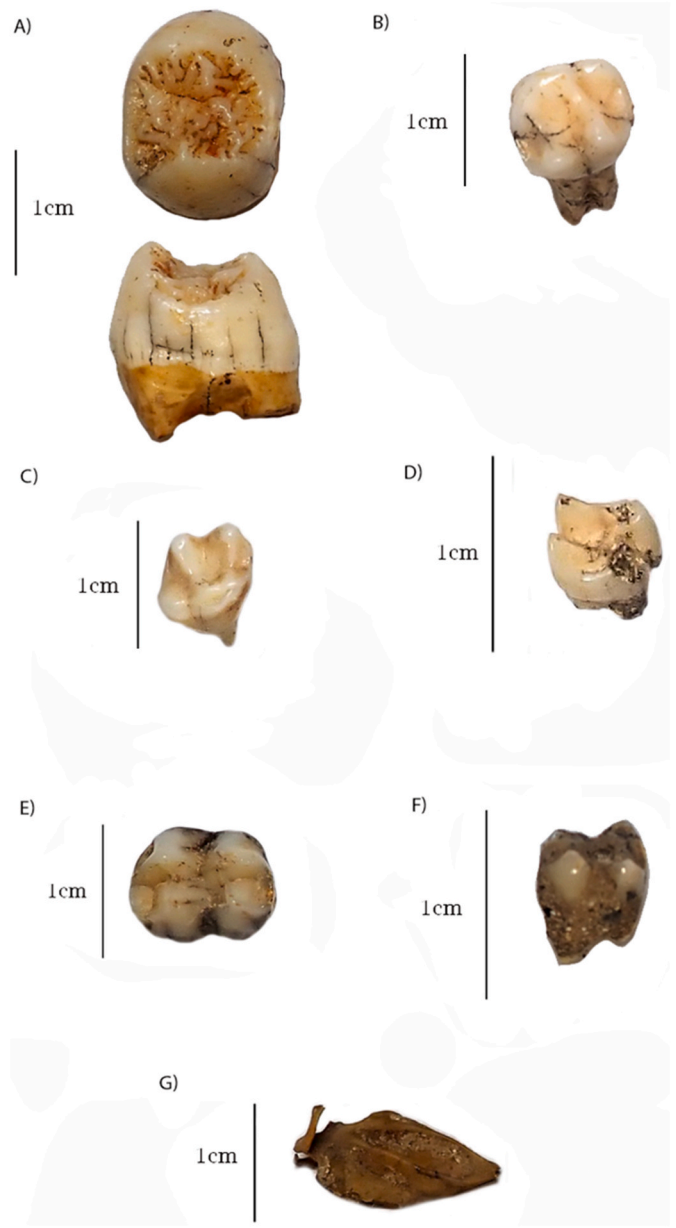

Fig. 6. (A) (above) NG11.20 *Pongo* sp., left P^3 occlusal view (below) and anterior view; (B) NG21.19 *Symphalangus*, left M^1; (C) *Hylobates*, right M^1; (D) NG13.14 *Presbytis*, right M^3; (E) GG1.10 *Nasalis*, left m_2; (F) NG20.10 *Macaca*, m_3; NG21.18 (G) NG34.14 Chiroptera, scapula.

Comparable morphology is seen in Pleistocene Southeast Asian specimens (Schwartz et al., 1994; Drawhorn, 1994; Bacon et al., 2001; Harrison et al., 2014; Filoux et al., 2015; Filoux and Wattanapituksakul, 2019). The tooth (15.11 mm in length and 12.26 mm in width) is larger than the average profile of modern *Pongo* specimens from Southeast Asia (Hooijer, 1948; Table S5), and towards the upper range of orangutan premolars recovered from other Pleistocene deposits in Sumatra (Hooijer, 1948). The taxonomy of fossil species is complicated for Sumatran *Pongo*, and so *Pongo* remains are not here assigned to species. Modern species that may be represented in the Ngalau Gupin collection include *Pongo abelii* (Lesson, 1827), and *Pongo tapanuliensis* (Nater et al., 2017).

Family: Hylobatidae Gray, 1870
Genus: *Symphalangus* Gloger, 1841
Species: *Symphalangus syndactylus* Raffles, 1821

Symphalangus syndactylus
Representative Specimen: NG21.19 – left M^1 – NG-B assemblage

(Fig. 6B)

NG21.19 is a first molar with four low, narrow reduced cusps. A prominent crista obliqua connects the protocone and metacone, with the ridge terminating lingually to the protocone. The paracone is wider than the protocone and the cusps are obliquely arranged, meaning that they form a rhombus, whereas in a lower second molar the anterior cusps would more-or-less form a square. The teeth excavated from this sample are too large to be considered *Hylobates agilis*; the gibbon found at Lida Ajer cave in the Padang Highlands (Hooijer, 1948, 1960). The dimensions of this sample fit well within the range of *Symphalangus syndactylus* from Southeast Asia (Hooijer, 1960; Frisch, 1967; supplementary Table S5).

Genus: *Hylobates* Illiger, 1811
Hylobates sp.
Representative Specimen: NG21.18 – right M^1 – NG-B assemblage

(Fig. 6C)

NG21.18 is an enlarged, broad crown that is marginally compressed laterally. This tooth is distinguished as a *Hylobates* molar due to the characteristic hypocone as the highest cusp, with the tooth wider than it is long (Hooijer, 1960). The dimensions of the tooth are within the range of the *Hylobates* from Southeast Asia (Hooijer, 1960; Frisch, 1967; supplementary Table S5).

Family: Cercopithecidae Gray, 1821
Subfamily: Colobinae Jerdon, 1867
Genus: *Presbytis* Eschscholtz, 1821
Presbytis sp.

Representative specimen: NG13.14 –right M^3 – NG-B assemblage
(Fig. 6D)

The overall morphology is typical of cercopithecine third molars, but this tooth has a critical characteristic that differs significantly in Presbytis from all other Asian colobines; the distal cusps are joined with no separation between crests (Willis and Swindler, 2004). The size range (6.1 mm in length and 5.29 mm in width) overlaps with the average profile for *Presbytis* molars (Swindler, 2002).

Genus: *Nasalis* St Hilaire 1812
Nasalis sp.
Representative Specimen: GG1.10 – left m_2 – NG-A assemblage

(Fig. 6E)

GG1.10 can be categorised as a left lower second molar of *Nasalis* due to the greater integration of the transverse lophs and less pronounced trigonid in comparison to other Old World Monkeys (Swindler and Orlosky, 1974). The tooth is stout and rounded with a bilophodont structure, and four highly pointed cusps that rapidly decline into a deep valley across the occlusal surface. The most pronounced cusp is the hypoconid, followed by the protoconid, the paraconid and finally the stout metaconid.

Subfamily: Cercopithicinae Gray, 1821
Genus: *Macaca* Lacépéde, 1799
Macaca sp.
Representative Specimen: NG20.10 – m_3 – NG-B assemblage

(Fig. 6F)

The third molar crown of NG20.10 is bilophodont with four sharp high cusps with a prominent distoconulus. There is a narrow groove running from the base of the cusps to the terminus of the enamel on the lingual and buccal surfaces of the molar. This specimen is identifiable as a *Macaca* molar due to the significant lingual groove; deeply defined to half of the width of the tooth, terminating at a perpendicular intersection with a small enamel ridge outlining the central tooth basin (Kay, 1978; Teaford, 1982). The four cusps of the molar are more prominent than those of the more derived molars of *Pongo*. Unlike the oblique arrangement of the *Symphalangus* molars, the cusps form a large square in occlusal view.

Order: Rodentia Bowdich, 1821
Family: Hystricidae Fischer de Waldheim, 1817
Genus: *Hystrix* Linnaeus, 1758
Hystrix sp.
Representative Specimen: NG3.38 – lower incisor – NG-B assemblage

(Fig. 5E)

The characteristic chisel-like shape and triangular cross-section with a slightly convex shape of NG3.38 are consistent with *Hystrix* lower incisors (e.g. Van Weers, 2005). The striking similarities in morphology between species (Van Weers, 2005; Monchot et al., 2012) and the overlap of the Ngalau Gupin specimens with the dimensions of the modern and extinct species from museum collections preclude specific diagnoses at this stage.

Order: Chiroptera Blumenbach, 1779
Representative Specimen: NG34.14 – right scapula – NG-B assemblage

The bone specimen NG34.14 is a right scapula. The scapula of Chiroptera have a distinctive morphology, including a reduced acromion process, a single articular surface and a globular glenoid cavity (Schlosser-Sturm and Schliemann, 1995; Panyutina et al., 2013).

Order: Artiodactyla Owen 1848
Family: Suidae Gray, 1821
Genus: *Sus* Linnaeus, 1758
Sus scrofa Linnaeus, 1758
Representative Specimen: NG30.10 – right M^3 – NG-B assemblage

(See Fig. 7, Fig. 7A)

The molar NG30.10 has very typical features of a suid: tall rounded bunodont cusps and numerous enamel projections creating an irregular occlusal surface (Cucchi et al., 2009; Berkovitz and Shellis, 2018). This molar is assigned to *Sus scrofa* on the basis of its relatively short and wide shape, with no obvious heptaconule. See supplementary Table S6 for the dimensions of suid teeth in the Ngalau Gupin collection.

Sus barbatus Müller, 1838
Representative Specimen: NG30.12 – right M^3 – NG-B assemblage

(Fig. 7B)

The molar is morphologically similar to that of *Sus scrofa* but is distinguished by the rugose enamel on the molar and the presence of bulky accessory tubercles most consistent with those of *Sus barbatus*, whereas tubercles in other suids are typically lacking (Tougard, 1998). This tooth falls within the size range of teeth taxonomically assigned to *Sus cristata* and *Sus barbatus* from Duoi U'Oi, Vietnam (Bacon et al., 2008; See supplementary Table S6). The considerable overlap in size makes identification difficult.

Family: Hippopotamidae Gray, 1821
Genus: *Hexaprotodon* Falconer and Cautley, 1836
Hexaprotodon sp.
Representative Specimen: GG4.1 – left m_2 – NG-A assemblage

(See Fig. 8)

Hexaprotodon has been identified using variations in cranial and skeletal features between recent and fossil species and considered to be a

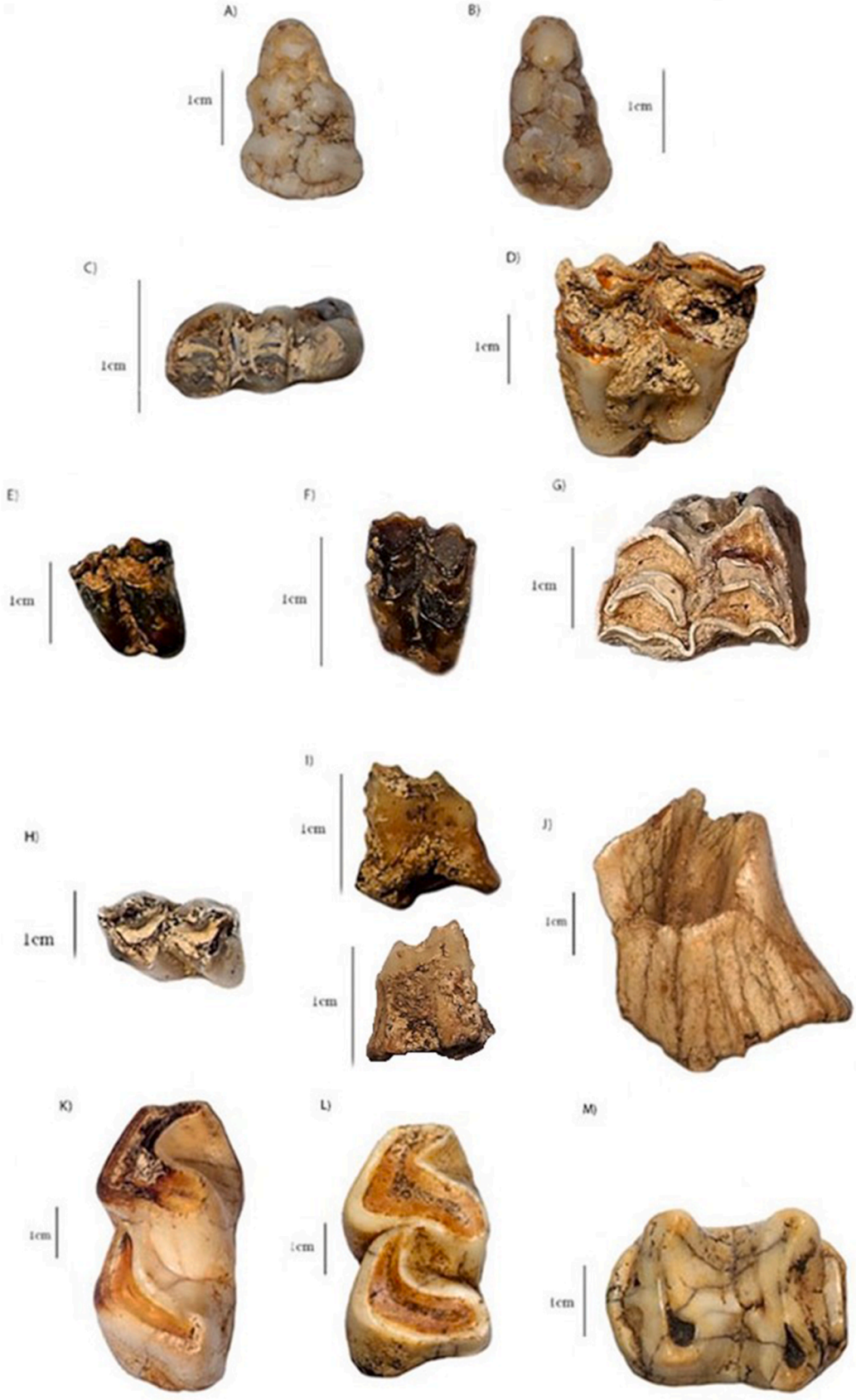

Fig. 7. (A) NG30.10 *Sus scrofa*, right M^3; (B) NG30.12 *Sus barbatus,* right M^3; (C) GG3.120 Tragulidae, m_3; (D) GU1 *Rusa* sp., left M1 from ex-situ deposits; (E) NG37.22 Cervidae, right M1; (F) NG32.18 *Muntiacus* sp., right M; (G) NG37.15 Bovidae, left M^3; (H) NG32.16 *Capricornis sumatraensis,* left m_2; (I) NG21.27 Moschidae, right P^4; (J) NG23.10 *Rhinoceros unicornis,* left M^1 fragment; (K) NG24.11 *Rhinoceros sondaicus,* left m_2; (L) NG24.10 *Dicerorhinus sumatrensis,* right m_2; (M) NG22.10 Tapiridae, right m_3.

Fig. 8. (Left) GG4.1 *Hexaprotodon* molar fragment; (right) modern *Choeropsis liberiensis* m2 from American Natural History Museum 81899 collection for comparison.

peculiar lineage of hippopotamids in Asia (Falconer and Cautley, 1836; Lydekker, 1884; Colbert, 1935; Hooijer, 1950; Coryndon, 1970, 1977; Boisserie and White, 2004). Specimen GG4.1 consists of the anterior portion of a left m_2, which preserves the protoconid, metaconid, and a well-developed anterior cingulid. It is well worn with the cusp apices absent, and significant dentine exposed. It is most comparable to specimen 81899 of *Choeropsis liberiensis* from the American Museum of Natural History, which are similarly worn (Fig. 4). Specimen GG4.1 is slightly larger than AMNH81899, with a more anteriorly orientated metaconid, a wider and more prominently defined anterior cingulid that forms a wider and more deeply developed anterolingual basin between the anterior margin of the protoconid and the posterior lobe of the anterior cingulum.

Family: Tragulidae Milne-Edwards, 1864
Representative Specimen: GG3.120 – right m3 – NG-A assemblage

(Fig. 7C)

This specimen is identifiable as there are four sickle-shaped cusps on the crown of the molar show a characteristic bunoselenodont morphology (Rössner, 2007). Moreover, this tooth can now be identified as a lower molar of a Tragulidae due to the characteristic well-developed ectostylid and by far the largest cusp is the hypoconid, which projects rostrally (Farooq, 2008). This specimen cannot be identified to genus level as wear of the surface morphology has removed any evidence of the characteristic 'tragulus fold' in the basin of the pre-hypocristid.

Family: Cervidae Linnaeus, 1758
Genus: *Rusa* Kerr, 1792
Rusa sp.
Representative Specimen: GU1 – left M^1 – NG-B assemblage

(Fig. 7D)

This cervid tooth is much larger than the specimen described previously, with the maximum length of 23.94 mm and width of 24.67 mm taken at the base of the specimen crowns. These measurements compare best with that of *Rusa unicolor* but this taxonomic assignment cannot be confirmed. This tooth has a pronounced entostyle. The tooth has the typical features of a *Rusa* molar; a notably brachyodont crown composed of four main cusps with sharp lingual crests in two lophs (Leslie, 2011). The tooth is a first molar, evident as the accessory elements such as the mesial and distal cingulum and entostyle are notably weak, and the postcingulid and *Palaeomeryx*-fold are absent (Dong and Chen, 2015).

Genus: *Muntiacus* Martin, 1886
Muntiacus sp.
Representative Specimen: NG32.18 – right M – NG-B assemblage

(Fig. 7E)

NG32.18 is a square tooth with four crescentic cusps. The tooth has a rectolinear hypocone and rounded protocone. It displays a distinct and well-developed mesostyle that wedges into a more reduced, thinner parastyle. It displays a thick, crenulated cingulum. The fossa is obscured by matrix.

Cervidae gen et sp. indet.
Representative Specimen: NG37.22 –right M^1 – NG-B assemblage

(Fig. 7F)

NG37.22 is attributable to Cervidae due to the distinct selenodont morphology with broad cingulum and steeply sloped sides of the crowns (Hillson, 2016). It is a rectangular tooth and attributed as a first molar due to the more lingually protruding protocone relative to the hypocone. These morphological characteristics and the small size of the tooth suggest that this may be a Muntjak molar, though this cannot be confidently established.

Family: Bovidae Gray, 1821
Representative Specimen: NG37.15 – left M^3 – NG-B assemblage

(Fig. 7G)

The NG37.15 tooth attributed to a bovid is robust with pronounced and pointed styles, particularly the metastyle. The hypocone and protocone protrude lingually together but are split down the middle, producing a "W" shaped outline (Hillson, 2005). A developed metastylar wing in the tooth is similar to the specimens of *Naemorhedus sumatraensis* published in Tougard (1998) and Bacon et al. (2008), though this cannot be confirmed.

Genus: *Capricornis* Ogilby, 1836
Species: *Capricornis sumatraensis* Bechstein, 1799
Representative Specimen: NG32.16 – left m_2 - NG-B assemblage

(Fig. 7H)

The tooth is a hypsodont crown with smooth enamel, low depressed walls and a single infundibulum (Hooijer et al., 1958; Wattanapituksakul et al., 2018). The crown has narrow central fossa bounded by a ridged hypoconid and protoconid. The hypoconid is far more pronounced than that of the protoconid, and there is no evident ectostylid (Suraprasit et al., 2016).

Family: Moschidae Gray, 1821
Moschus Linnaeus, 1758
Moschus sp.
Representative Specimen: NG21.27 –right P^4 – NG-B assemblage

(Fig. 7I)

This specimen is moderately molariform, alike to modern P^4 representatives (Zhang et al., 2018). However, the talonid of the specimen is broad and approximately triangle, and the metacone is orientated distally; characteristic of a P^4. The tooth is selenodont with a well-developed but low crown, and high column-shaped flat lingual walls. The crown has a shallowly depressed central fossa enclosed by a prominent anterior metastyle and parastyle, and a posterior protocone. The anterior styles have much higher dimensions than the posterior of the crown.

Order: Perissodactyla Illiger, 1811
Family Rhinocerotidae Gray, 1820
Genus *Rhinoceros* Linnaeus, 1758
Rhinoceros unicornis Linnaeus, 1758
Representative Specimen: NG23.10 –left M^1 fragment - NG-B assemblage

(Fig. 7J)

The specimen is a posterior buccal fragment preserving the hypocone, partial metaloph, postfossette and posterior cingulum. A steep partial metaloph dips immediately into a deep, narrow concave postfossette, with the exterior lip of the postfossette descending broadly into a partial metaloph. The specimen has a V-shaped and considerably deep molar valley, which combined with its large size, suggests this tooth is attributable to *Rhinoceros unicornis* (Guérin, 1980; Laurie et al., 1983; Groves, 1983).

Rhinoceros sondaicus Desmarest, 1822
Representative Specimen: NG24.11 –left m_2 – NG-B assemblage

(Fig. 7K)

This second molar is identified as Rhinocerotidae as it displays the classic pair of U-shaped lophs (Tong and Guérin, 2009). It is distinguished from *Dicerorhinus* on the basis of relatively equal depths of the molar valleys (Groves, 1983; Tong and Guérin, 2009), and excluded from *Rhinoceros unicornis* on the basis of its smaller size (Guérin, 1980).

Genus: *Dicerorhinus* Gloger, 1841
Dicerorhinus sumatrensis Fischer, 1814
Representative Specimen: NG24.10 –right m_2 – NG-B assemblage

(Fig. 7L)

The tooth of Dicerorhinus sumatrensis is morphologically like that of Rhinoceros sondaicus. The features that distinguish the teeth of these species are subtle; the medial valley (trigonid pit) is much shallower than the distal valley (talonid pit) (Groves, 1983; Tong and Guérin, 2009).

Family: Tapiridae Gray, 1821
Genus: *Tapirus* Brünnich, 1772
Species: *Tapirus indicus* Desmarest, 1819
Representative Specimen: NG22.10 – right m_3 – NG-B assemblage

(Fig. 7M)

This molar of the Tapiridae is easily identifiable due to the characteristic brachydont low crowns with two distinct lophs separated by a long, straight traverse ridge (Hooijer, 1947b). The tooth is likely a third molar, evident as the talonid and trigonid are more or less equal, with a well-developed anterior cingulid. The dimensions of this specimen fall well within the morphology and size range for *Tapirus indicus* (Desmarest, 1819; Hooijer, 1947b; Tong, 2005; supplementary Table S7).

Order: Carnivora Bowdich, 1821
Family: Felidae Fischer de Waldheim, 1817
Subfamily: Felinae Fischer de Waldheim, 1817
Representative Specimen: NG15.17 – right m_1 – NG-B assemblage

(See Fig. 9, Fig. 9A)

The singular first molar is divided solely into two broad protoconid and paraconid blades. The protoconid diverge minimally towards the labial, and the paraconid diverges minimally towards the lingual, and these two conids converge at a short deep groove buccally. There is a shallow broad depression on the occlusal surface extending at a shallow angle from the tip of the conid blades. There is no evident metaconid or talonid on this tooth. This tooth morphology and size profile could plausibly fit the size profile of the three common feline species in Sumatra: the Asian Gold Cat (*Pardofelis temminckii*), the Marbled Cat (*Pardofelis marmorata*) and the Leopard Cat (*Prionailurus bengalensis*) (Sunquist and Sunquist, 2009; Francis, 2017).

Genus: *Panthera* Oken, 1816
Representative Specimen: NG15.11 – left p_3 – NG-B assemblage

(Fig. 9B)

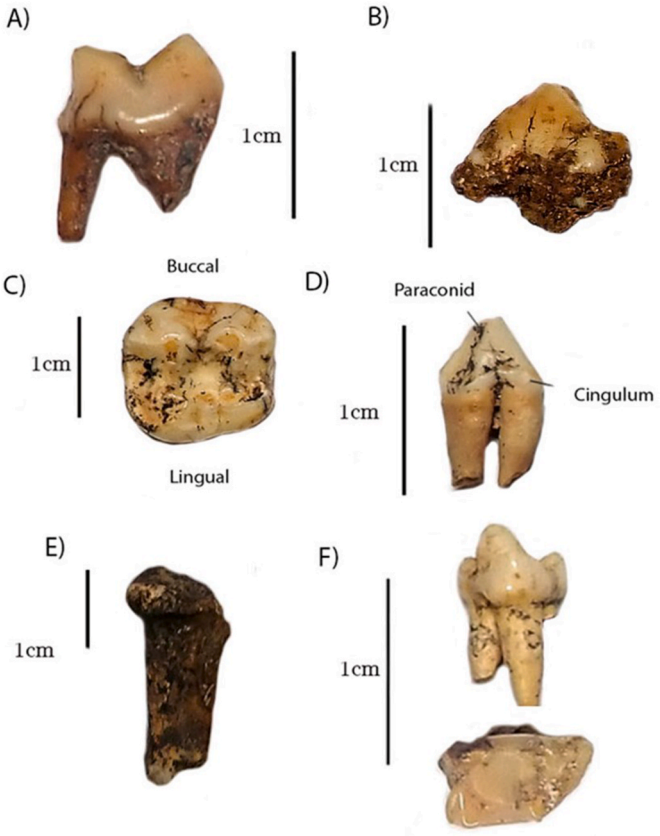

Fig. 9. (A) NG15.17 Felid, right m_1; (B) NG15.11 *Panthera tigris,* left p_3; (C) NG26.10 *Helarctos*, right M^1; (D) NG15.28 Mustelid, right p_4; (E) NG1.2 Viverridae, calcaneum; (F) (left) NG15.26 *Paradoxurus*, right m_1, disto-lingual view; (right) NG15.26 *Paradoxurus,* right m_1 occlusal view.

This specimen has the morphology of a third lower premolar (Hillson, 2005). There is a blunted protoconid with a main shearing crest, a small mesial paraconid and a small distal hypoconid that fit the morphology of a feline lower third premolar (Hooijer, 1947a). NG15.11 premolar conforms to the standard size variance best fits that of the *P. tigris* (Hooijer, 1947a; Badoux, 1959; Mazak, 1981; supplementary Table S8).

Family Ursidae Fischer de Waldheim, 1817
Genus *Helarctos* Raffles, 1821
Representative Specimen: NG26.10 – right M^1 – NG-B assemblage

(Fig. 9C)

This tooth is a broad, flat bunodont crown. It is nearly square in shape; a broad transverse valley separates the metacone and paracone from the lower protocone. The metacone and paracone are higher than that of the protocone. The mesial and distal edge of the metacone and paracone pinch into a small ridge. A deep notch separates the protocone and metacone. This molar conforms to those of the modern *Helarctos* (Raffles, 1821), and those excavated from similar cave sites in the region (Hooijer, 1948; de Vos, 1983; Long et al., 1996; Christiansen, 2008; supplementary Table S8).

Family: Mustelidae Fischer de Waldheim, 1817
Subfamily: Mustelinae Fischer de Waldheim, 1817
Representative Specimen: NG15.28 – right p_4 – NG-B assemblage

(Fig. 9D)

NG15.28 is a triangular monocuspid tooth with a sizeable pointed paraconid. This conid steeply slopes down to a stout shallow talonid

basin surrounded by a prominent cingulum. These features are characteristic of a lower right fourth premolar of Mustelidae, though the dimensions overlap with numerous individuals and so cannot be determined to genus level (Popowics, 2003; Hillson, 2005; Peigné et al., 2009; Grohé et al., 2010).

Family: Viverridae Gray, 1821

Representative Specimen: NG1.2 – left calcaneum – NG-B assemblage

(Fig. 9E)

The specimen is a small calcaneum. The features distinctive of Viverridae are prominent and pointed sustentaculum tali at almost a right angle to the neck of the calcaneum and the process calcaneus is robust and square, with a distinct groove on the plantar surface (Stains, 1983).

Genus: *Paradoxurus* Cuvier 1822

c.f. *Paradoxurus* sp.

Representative Specimen: NG15.26 – right m_1 – NG-B assemblage

(Fig. 9F)

This bunodont tooth has a triangular outline in occlusal view. The buccal cusps are stout and rounded, with a reduced protoconid, large, bulbous paraconid, a well-developed, rounded metaconid, a bulbous cusp-like parastylid, with a small, poorly-developed metaconulid located in the valley between protoconid and paraconid. The paraconid is the highest cusp. The tooth lacks a distinct buccal cingulum. The tooth NG15.26 most resembles the modern palm civet (Gregory and Hellman, 1939; Popowics, 2003) and is tentatively identified as *Paradoxurus*.

4.2. U-series and ESR dating

4.2.1. ESR dose evaluation

The five samples measured by ESR are characterised by relatively weak ESR intensities, especially for the least irradiated aliquots, which is why acquisitions of up to 50 scans have been performed. However, many ESR spectra still show a non-horizontal baseline and low signal-to-noise ratio (<5), both of which may significantly bias the D_E evaluation. Consequently, a cubic baseline correction was employed for all ESR spectra as in Duval and Martín-Francés (2017), before extracting the T1-B2 ESR intensity. Additionally, the mean scan-normalized noise ESR intensity extracted from all the aliquots of a given sample measured at a given time was subtracted from the intensity of the radiation-induced ESR signals. Final D_E evaluation was performed using the baseline- and noise-corrected ESR intensities (Table S3 and Figure S1).

Measurement precision achieved is overall excellent, with all samples showing a variation of <2.5%. This results in a D_E repeatability that is systematically <5%, with the exception of SUM18-26 (6.4%). D_E values range between 20 and 40 Gy (Gy). Consequently, the dose-response curve of each sample was restricted to D_{max}/D_E ratios of between 5 and 10, in accordance with the recommendations of Duval and Grün (2016) (see Supplementary Information Table S3). This restriction on the maximum applied irradiation dose (D_{max}) has, however, only a very limited impact on the D_E estimates: they vary between −2% and +5% when considering the full dose range instead - but remain systematically within 1-σ consistent (Figure S1). No apparent D_E pattern is observed for the two loci: D_E estimates range from ~22 to ~35 Gy for NG-A teeth, while the two NG-B teeth provide very close results around 32–34 Gy.

4.2.2. Solution U-series analyses

4.2.2.1. Bulk analyses of dental tissues. U-series results associated with the ESR analyses are displayed in Table 1. 230Th/232Th ratios measured in all dental tissues are systematically >30, which indicates that contamination by detrital Th is minimal and has a very limited impact (<2%) on the apparent U-series ages. Enamel tissues show mostly very low uranium concentrations between 0.04 and 0.11 ppm; these samples yield apparent U-series ages ranging from between ca. 50 and 60 ka, except for sample SUM18-24, which displays a much older estimate of about 90 ka. Dentine tissues show higher concentration values that vary within a narrow range (3.37–5.28 ppm). The apparent U-series ages are systematically younger compared with the enamel layer from the same tooth, between 28.6 and 48.9 ka. This different age pattern between is reinforced by the initial 234U/238U ratio calculated for each sample: it varies between 1.071 and 1.110 for the dentine samples and 1.208–1.390 for the enamel, suggesting that enamel and dentine may have experienced different uranium uptake processes. The dentine being usually more sensitive than enamel to any geochemical/diagenetic changes in the surrounding environment, we suspect that dentine tissues may have been impacted by a more recent U uptake event. Without spatially resolved U-series data, it is, however, currently impossible to draw any further conclusion from the present data set.

Interestingly, the U-series data collected for fossil teeth from NG-A and NG-B show a slightly different pattern: enamel tissues from NG-B return the oldest U-series ages in comparison with those from NG-A (61–91 ka vs. 52–59 ka), and similar observations can be made for the dentine tissues (45–49 ka vs. 28–42 ka).

4.2.2.2. U concentration and age profiling for GG4.1. We also produced five independent U-series ages for the *Hexaprotodon* specimen GG4.1 (Table 2). Uranium concentration is lowest for the enamel (ca. 2 ppm) but also yielded the oldest 230Th age (ca. 85 ka). The dentine portions contained a higher concentration of uranium (ca. 7–13 ppm) and systematically lower ages of ca. 76–73 ka, like the other dated samples above. Similarly, there are high 230Th/232Th activity ratio suggesting that detrital contaminants do not substantially affect the uncorrected versus corrected ages.

GG4.1 differ from the other dated teeth in many aspects. For example, the apparent U-series ages in the dentine are systematically younger than those measured in the other teeth (Table 1). Similarly, measured and initial 234U/238U activity ratios are lower, which may suggest a different uptake history and/or geochemical environment for this specimen. The tooth is not ideal for U-series dating given the variability in uranium concentration through the tooth, especially the dentine. This variability might also partly explain the reason for such distinct U-series data among the teeth. However, several ages of GG4.1 dentine are clustered around 68–72 ka. There may be multiple phases of U-uptake in the tooth, but there is no clear evidence of U-leaching. We are confident that the tooth has produced reliable minimum ages of around 56–73 ka. Significantly this age interpretation is consistent with other teeth dated with the combined U-series/ESR approach detailed below.

4.2.3. Combined U-series and ESR age calculations

Among all the initial ESR age calculations (samples labelled “a” in Table 1), only one sample (SUM18-21a) returned a finite combined US-ESR age result (134 + 12–11 ka). A very close CSUS-ESR estimate of 141 ± 13 ka was obtained for this tooth, which indicates that the modelling of uranium uptake into dental tissues has a negligible impact on the calculated age. This is due to the limited contribution of dental tissues to the total dose rate (about 13%).

Initial combined US-ESR age calculations did not return results for the other samples (SUM18-22a, SUM18-24a, SUM18-26a, SUM18-27a), suggesting thus that dental tissues may have experienced uranium leaching. This is confirmed by the finite AU-ESR ages obtained for all of them. In particular, the other two teeth from NG-A (SUM18-26a and SUM18-27a) yield much younger age estimates of around 40–50 ka compared with SUM18-21a. However, AU-ESR, EU-ESR and CSUS-ESR estimates are systematically within error for all samples, indicating

Table 2
U-series isotopic data for GG4.1 *Hexaprotodon* molar from Ngalau Gupin, Sumatra (errors are 2σ).

Sample	U (ppm)	232Th (ppb)	230Th/232Th	230Th/238U	234U/238U	uncorr. 230Th Age (ka)	corr. 230Th Age (ka)	corr. Initial (234U/238U)
HIP-1 (enamel)	1.977 ± 0.002	19.2 ± 0.1	193 ± 2	0.618 ± 0.004	1.122 ± 0.002	85.5 ± 0.8	85.3 ± 0.8	1.156 ± 0.002
HIP-2 (dentine)	6.94 ± 0.04	102 ± 1	103 ± 1	0.50 ± 0.01	1.067 ± 0.006	68.4 ± 1.5	68.0 ± 1.5	1.081 ± 0.007
HIP-3 (dentine)	9.72 ± 0.04	1.25 ± 0.04	10272 ± 338	0.44 ± 0.01	1.080 ± 0.004	56.1 ± 0.9	56.1 ± 0.9	1.094 ± 0.005
HIP-4 (dentine)	12.52 ± 0.01	18.1 ± 0.1	1077 ± 8	0.514 ± 0.003	1.096 ± 0.002	68.3 ± 0.6	68.2 ± 0.6	1.117 ± 0.003
HIP-5 (dentine)	12.32 ± 0.01	13.0 ± 0.1	1544 ± 13	0.539 ± 0.003	1.097 ± 0.002	72.8 ± 0.7	72.7 ± 0.7	1.119 ± 0.002

Note: Ratios in parentheses are activity ratios calculated from the atomic ratios, but normalized to measured values of secular-equilibrium HU-1 Pike et al. (2002). All errors are given at the 2σ level. 230Th ages are calculated using Isoplot EX 3.0 (Ludwig, 2003) with decay constants $\lambda_{238} = 1.551 \times 10^{-10}$ yr^{-1} (for 238U), $\lambda_{234} = 2.826 \times 10^{-6}$ yr^{-1} (for 234U) and $\lambda_{230} = 9.158 \times 10^{-6}$ yr^{-1} (for 230 Th), respectively (Cheng et al. 2000). 2σ errors in the uncorrected (uncorr.) ages were propagated directly from the uncertainties in the (230Th/238U) and (234U/238U). The corrected (corr.) 230Th age was calculated using the assumed bulk earth or upper crust value equivalent to the detrital 230Th/232Th activity ratio of 0.83 (Cheng et al., 2000; Pike et al., 2002; Ludwig et al., 2003).

that the potential occurrence of uranium leaching, or any other types of uranium uptake, has only a minimum influence on the calculated ESR results. This is because the dose rate is dominated by the contribution from the sediment. When considering both beta and gamma dose rate components coming from sediment sample SUM18-11 (scenario b), the resulting US-ESR age for SUM18-21b gets much younger by a factor >2 (57 +5–4 ka) and becomes consistent with SUM1826a & SUM18-27a (Table 1). A somewhat similar observation can be made when using the sediment attached to SUM18-21 instead: all ages get much older, SUM18-21a and SUM18-26b being consistent (134 vs 130 ka), while SUM18-27b is younger by about 30 ka, but nevertheless 2σ consistent. This tooth displays the smallest D_E of the data set (15% and 37% lower than SUM18-21 & SUM18-26), which might be due to a locally less radioactive environment around the tooth in comparison with the other fossils. The significant age gap between scenario a and b for NG-A samples is simply due to the massive difference in the gamma dose rate derived from sediment associated to SUM18-21 (173 ± 14 Gy/a) and SUM18-11 (460 ± 35 Gy/a). Since SUM18-21a is the only tooth for which the original sediment attached to the tooth was collected, we may reasonably consider it as being the most reliable age estimate for NG-A, and it is possible that sediment SUM18-11 has been collected from a locally weathered breccia within NG-A and may thus not provide an accurate estimate of the true gamma dose rate. The very similar radioactivity levels measured in SUM18-11 and SUM18-12 from NG-B, and

Table 3
The representation of each taxa in NISP of the NG-A and NG-B assemblages.

Class	Order	Family	Taxon	Common name	NG-A NISP	NG-B NISP
Reptilia	Squamata	Varanidae	gen. et sp. indet.	Lizard	0	1
Aves	gen. et sp. indet.	gen. et sp. indet.	gen. et sp. indet.	Bird	0	3
Mammalia	Artiodactyla	Suidae	*Sus* sp.	Pig	23	77
			Sus scrofa	Crested pig	12	43
			Sus barbatus	Bearded pig	13	18
		Hippopotamidae	*Hexaprotodon*	Pygmy Hippo	1	1
			gen. et sp. indet.	Hippo	6	0
		Tragulidae	gen et sp. indet.	Mouse deer	1	0
		Cervidae	*Rusa* sp.	Sambar deer	0	4
			Muntiacus sp.	Muntjak	1	2
			gen et sp. indet.	Deer	4	43
		Bovidae	gen. et sp. indet.	Cow	4	11
			Capricornis sumatraensis	Serow	0	1
		Moschidae	gen. et sp. indet.	Mouse deer	0	1
	Primates	Hominidae	*Pongo* sp.	Orangutan	13	40
		Cercocipithedae	*Presbytis*	Surili	0	16
			Macaca sp.	Macaque	3	25
		Colobinae	*Nasalis* sp.	Proboscis monkey	1	0
		Hylobatidae	*Symphalangus syndactylus*	Siamang	0	19
			Hylobates sp.	Gibbon	0	2
	Perissodactyla	Rhinocerotidae	*Rhinoceros unicornis*	Indian rhino	0	1
			Rhinoceros sondaicus	Javan rhino	0	1
			Dicerorhinus sumatrensis	Sumatran rhino	0	3
			gen. et sp. indet.	Rhino	6	8
		Tapiridae	*Tapirus indicus*	Tapir	4	7
	Carnivora	Ursidae	*Helarctos*	Sun bear	2	6
		Felidae	gen. et sp. indet.	Wild cat	0	9
			Panthera	Tiger	1	7
		Mustelidae	gen. et sp. indet.	Mustela	0	3
		Viverridae	*Paradoxurus*	Palm civet	0	6
	Chiroptera	Microchiroptera	gen. et sp. indet.	Bat	5	13
	Rodentia	Hystricidae	*Hystrix* sp.	Porcupine	14	56
			gen et sp. indet.	Rat	0	3
	Proboscidea	Elephantidae	*Elephas* sp.	Elephant	1	2

the heavily weathered state of the breccia at NG-A, indirectly support this hypothesis.

Teeth SUM18-22a and SUM18-24a from NG-B return very close AU-ESR age estimates (60 ± 10 and 61 ± 2 ka). Although these results indicate that dental tissues have experienced uranium leaching, the uranium uptake modelling has only a very limited impact on the calculated ESR ages: EU-, AU- and CUS-ESR results are virtually the same (Table 1) for a given sample. Again, the dose rate is dominantly, and almost exclusively, driven by the external beta and gamma dose rate from the sediment. However, because the teeth were found at NG-B within the first 10 cm below ground surface, it may reasonably be considered that the infinite matrix assumption was not fulfilled, At a 10-cm depth, the tooth would receive about 88% of the gamma dose rate instead (Aitken, 1985). New age calculations based on this scenario (labelled "b" in Table 1), return results older by about 8 ka (+13%). Interestingly, a finite US-ESR age result of 68 + 7–6 ka (Table 1) may be obtained for SUM18-22b, while SUM18-24b yield ages of around 68 ka, whatever the uranium uptake model considered. We acknowledge that scenario b most likely underestimates the true dose rate: the contribution of the air component in the gamma dose rate is not null, as it may include a non-negligible contribution from the Rn gas present in the cave, and from the gamma-rays from the sediment that are reflected by the limestone wall. Consequently, the true gamma dose rate is most likely somewhere between the two values used for scenarios a and b. The resulting ages may bracket the true age of the fossils assuming they have not been reworked from other deposits.

4.3. Taphonomic analysis

4.3.1. Taxonomic representation

In the NG-A assemblage, a total of 141 fossils were recovered, representing 17 genera and a minimum of 26 individuals (Table 3). In the NG-B assemblage, a total of 1313 fossils were recovered, representing 30 genera and a minimum of 80 individuals. Both loci produced a diverse suite of small to large herbivorous, omnivorous, carnivorous and durophagous (bone feeding) animals. Mammals dominate both assemblages, and a small number of bird, reptile and mollusc remains were recovered from NG-B. The bird, reptile and mollusc remains were not included in the taphonomic analysis. Fifteen taxa are shared between the NG-A and NG-B assemblages (*Pongo*, *Macaca*, *Sus scrofa, Sus barbatus*, Rhinocerotidae, Cervidae, *Hexaprotodon, Muntiacus*, Bovidae, *Elephas*, *Helarctos, Hystrix*, *Tapirus indicus*, *Panthera tigris* and Chiroptera). Only two taxon are found exclusively in the NG-A assemblage (Tragulidae and *Nasalis*), while sixteen taxa were found exclusively in the NG-B assemblage (Felidae, *Rusa*, *Capricornis sumatraensis*, *Dicerorhinus sumatrensis*, *Rhinoceros unicornis*, *Rhinoceros sondaicus*, *Hylobates*, *Symphalangus*, *Presbytis*, *Paradoxurus*, Mustelidae, Rodentia, Varanidae, Viverridae, Moschidae and Aves; Fig. 10).

The representation of taxa in each deposit is provided in Tables 3–4 and Figure S2 & S3. In the NG-A assemblage, artiodactyls are the most abundant taxon (53.2% NISP), followed by primates (15.6% NISP), rodents (12.8% NISP), perissodactyls (10.1% NISP), bats (4.5% NISP), carnivores (2.8% NISP) and proboscideans (1% NISP). In the NG-B assemblage, artiodactyls are once again the most abundant (46.3% NISP), followed by primates (24.1% NISP), rodents (13% NISP), carnivores (7.6% NISP), perissodactyls (4.6% NISP), bats (3% NISP), birds

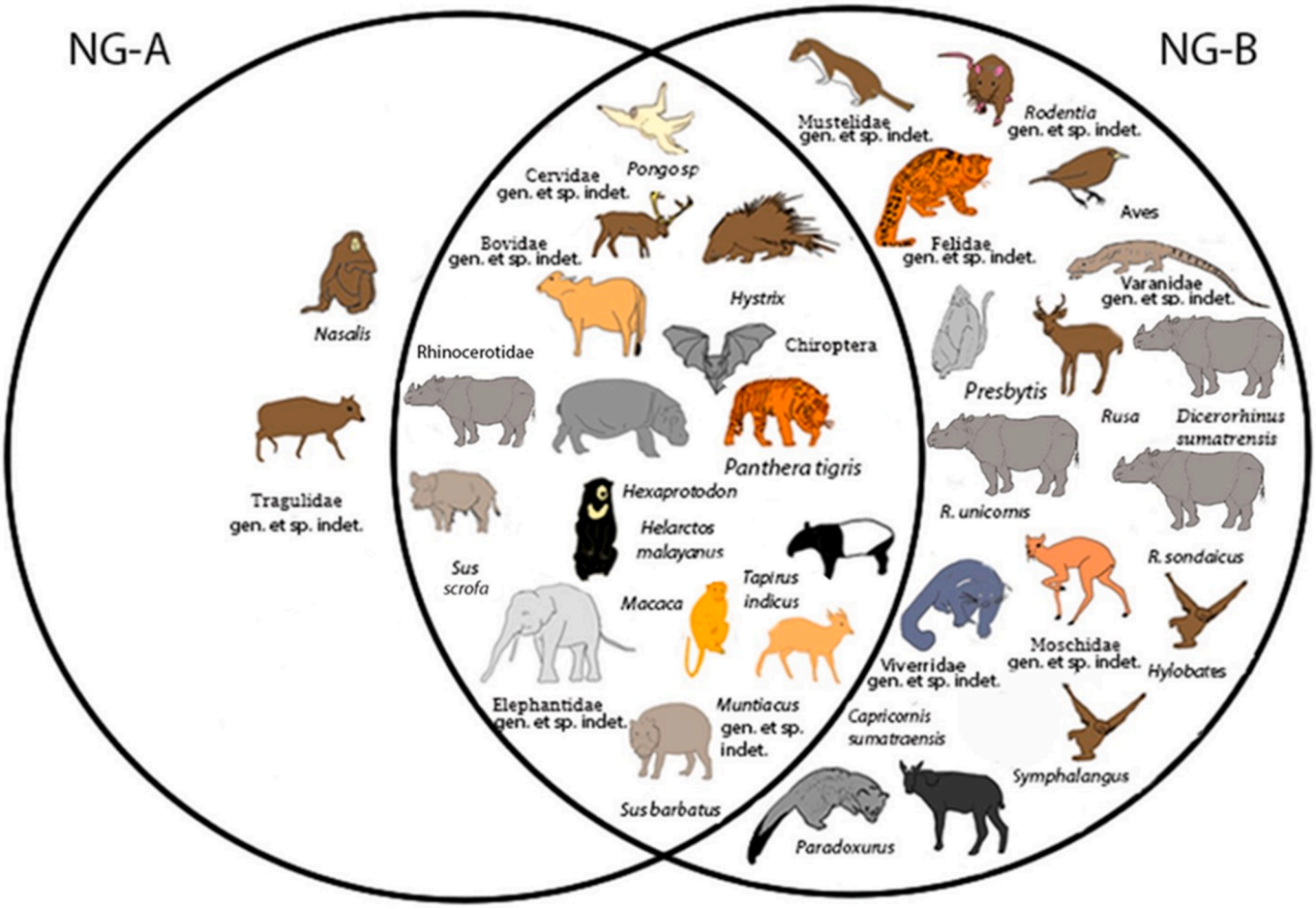

Fig. 10. Venn diagram of the relationship between the faunal representations in the NG-A and NG-B assemblages.

Table 4
Abundance of NISP of taxonomically identifiable teeth in the Ngalau Gupin collection according to taxon.

	NG-A molar NISP	NG-A premolar NISP	NG-A incisor NISP	NG-A canine NISP	NG-B molar NISP	NG-B premolar NISP	NG-B incisor NISP	NG-B canine NISP
Artiodactyl	22	16	3	2	107	61	9	5
Primates	12	1	1	1	49	26	15	6
Rodentia	4	0	5	3	42	8	21	0
Carnivora	1	2	0	0	8	18	0	0
Perissodactyl	1	2	0	1	12	2	0	0
Chiroptera	0	0	0	0	5	4	0	0
Total NISP	40	22	9	7	223	119	45	11

(0.7% NISP) and proboscideans (0.5% NISP) and varanids (0.2% NISP). There is no difference in mammalian NISP between the two deposits (X^2 (6, N = 97,99.1) = 7.01, p = 0.32).

The most abundant taxon classified in the identifiable tooth specimens of the NG-B assemblage are artiodactyls (n = 200, 48% of NISP), followed by primates (n = 102, 24.4% of NISP), rodents (n = 53, 12.7% of NISP), carnivores (n = 30, 7.2%), perissodactyls (n = 20, 4.9% of NISP) bats (n = 9, 2.1% of NISP) and finally proboscideans (n = 2, 0.5% of NISP). Based on identifiable teeth, taxa are similarly represented in the NG-A assemblage (X^2 (7, N = 104,416) = 13.137, p = 0.07), with artiodactyls being best represented (n = 58, 55.7% NISP), followed by primates (n = 17, 16.3% of NISP), rodents (n = 14, 13.5% of NISP), perissodactyls (n = 12, 10.6% of NISP), carnivores (n = 3, 3% of NISP) and proboscideans (n = 1, 1% of NISP) (Fig. 12).

Given their proximity and the significant overlap in represented taxa, an interpretation that the NG-B assemblage originated from the NG-A breccias is our null hypothesis. This hypothesis is consistent with the favoured interpretation of the ESR/U-series data suggesting the two deposits are of a similar age. The greater species richness in the NG-B assemblage could simply be explained by its larger sample size.

4.3.2. *Skeletal part representation*

Isolated bone and tooth fragments dominate and make up 98% (n = 117) and 63% (n = 539) of the NG-A and NG-B total assemblages, respectively. Only 29 complete bones were recovered: 24 from NG-B and five from NG-A. The surviving complete elements from NG-B comprise phalanxes (n = 6), vertebrae (n = 4), and radii (n = 3), followed by calcanei, metatarsals, and humeri (n = 2) and a single metacarpal, rib, tibia, clavicle and scapula. Identifiable skeletal fragments from NG-B include two partial mandibles, one partial maxilla, three partial vertebrae, 27 cranial fragments, three partial ribs and 38 long bone midshaft fragments. A single petrosal and four long bones attributed to the wings of Chiroptera were recovered from the NG-A breccias. All (n = 5) post-cranial elements in the NG-A deposit and 87.5% (n = 60) of those in the NG-B deposit belong to small mammals (e.g. bats, rodents, felids) and birds. Only three post-cranial remains from the NG-B assemblage can be assigned to larger mammals; a juvenile pig metatarsal and two primate phalanxes.

Teeth are abundant in both loci from Ngalau Gupin, and 87.4% (n = 104) and 72% (n = 417) of the dental material from the NG-A and NG-B deposits can be assigned to taxon. Molars, premolars, incisors, and canines make up 55% (n = 214), 30.6% (n = 119), 11.6% (n = 45), and 2.8% (n = 11) of all taxonomically identifiable teeth in the NG-B assemblage, and 50.6% (n = 40), 28.6% (n = 22), 11.7% (n = 9), and 9.1% (n = 7) of all taxonomically identifiable teeth in the NG-A assemblage (See Table 4 and Fig. 11). There is no statistical difference in the representation of tooth types between these the two deposits (X^2 (4, N = 389,77) = 4.54, p = 0.34), consistent with our null hypothesis.

4.3.3. *Bone breakage*

Most limb bone fragments in the NG-A assemblage exhibit right (n = 1, 6%), jagged (n = 3, 20%) and transverse (n = 5, 33%) fracture patterns consistent with fracturing of dry bones. Still, oblique (n = 5, 33%) and curved (n = 2, 13%) fracture patterns indicate that breakage also occurred while still fresh. Likewise, the NG-B long bones exhibit fracture patterns that indicate breakage occurred while the bones were fresh as well as dry. Many bones exhibit right (n = 21, 36.25%), jagged (n = 19, 49%) and transverse (25.5%, n = 11) fractures consistent with dry fracturing, while a number of oblique (27.5%, n = 16), smooth (n = 21, 51%) and curved (n = 11, 25.5%) fractures suggest fresh breakage of bones. Oblique/right (n = 21, 36.25%) and intermediate (n = 21, 49%) fractures were also recorded.

4.3.4. *Nature of accumulation*

There are no cut marks or intentional bone breakage, marks or modification, so we cannot relate the bone assemblage to human

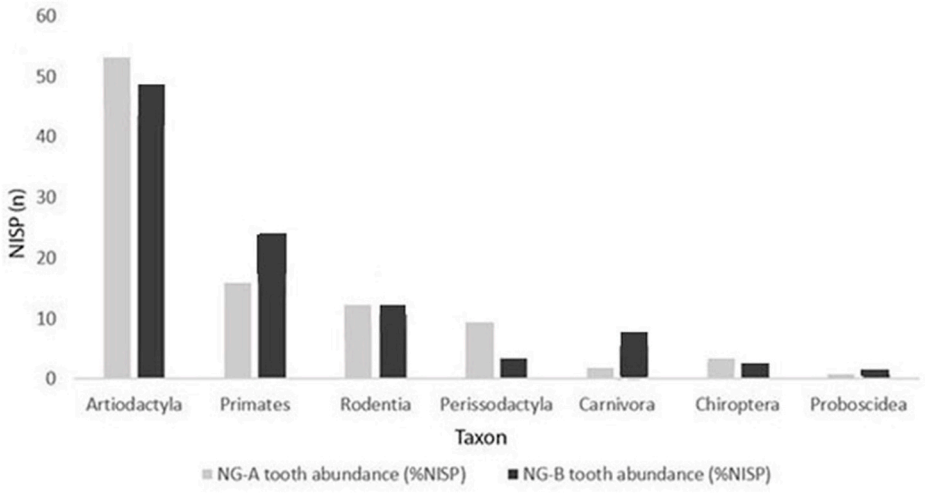

Fig. 11. The %NISP tooth abundance in each biological order of the NG-A and NG-B assemblages.

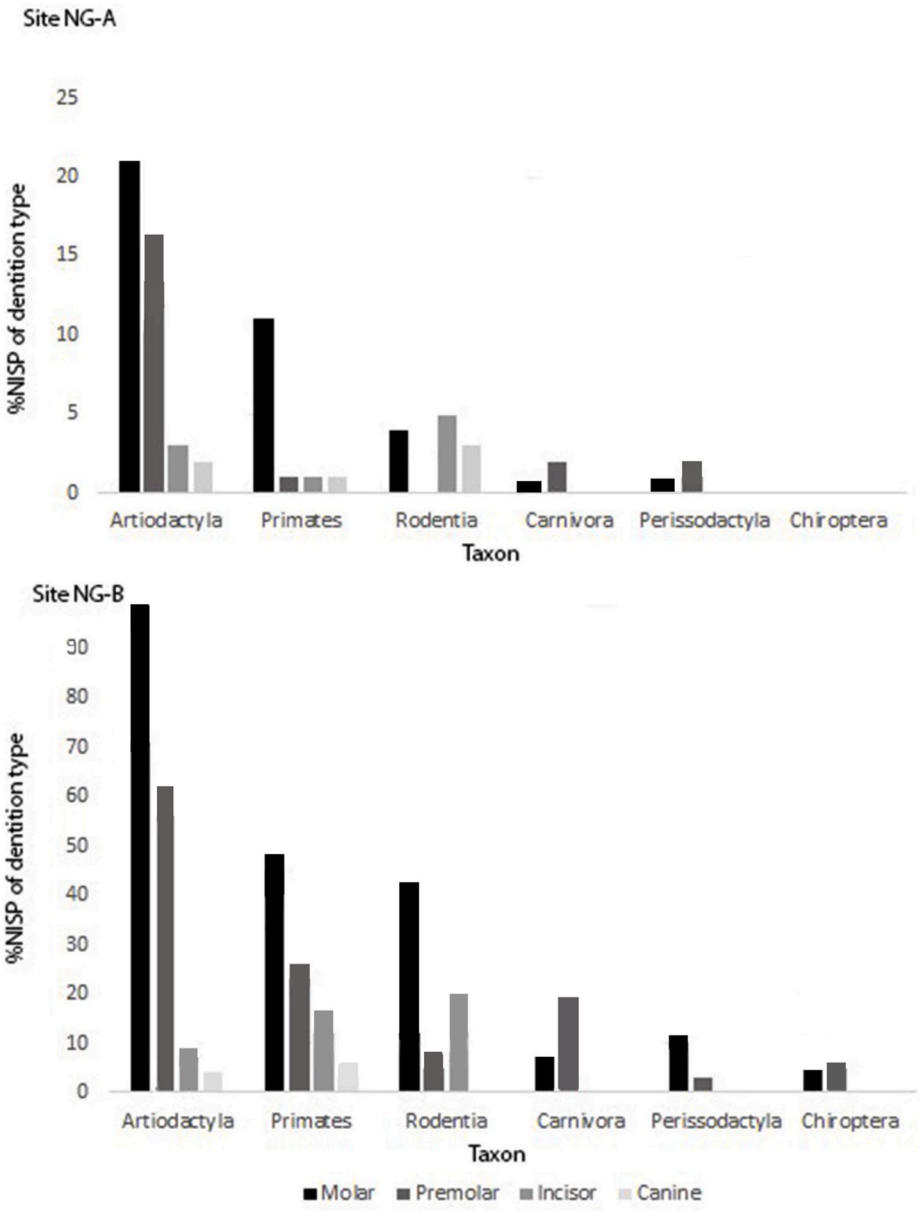

Fig. 12. The %NISP of each dentition type in each biological order of the NG-A and NG-B assemblage.

activities or bone collecting behaviours such as scavenging or hunting by humans nor stone tools. Three bones from loci NG-B exhibit marks that might be consistent with burning, but confirmation requires chemical testing not yet attempted. Nine species from Ngalau Gupin could theoretically have modified the assemblages: tigers (Brain, 1981; Haynes, 1983), porcupines (Thomas, 1971; Behrensmeyer and Hill, 1988), pigs (Olsen and Shipman, 1988), macaques (Sugiyama et al., 2009; De Marco, 2018), gibbons, felids (Andrés et al., 2012), palm civets, mustelids and rodents (Denys, 2002; Klippel and Synstelien, 2007; Pokines et al., 2017). A small blackened long bone fragment from the NG-B assemblage exhibits numerous small carnivore tooth pits and punctures across the midshaft (Fig. 13). These perforations average 1.1 mm in width and are prolific across the midshaft of the long bone. These perforations can be related to a small carnivore. There are numerous small carnivores present in the Ngalau Gupin deposits that are plausible agents for this damage, including mustelids, viverrids, felids, and varanids.

The second definitive biotic agent that can be confirmed in the Ngalau Gupin collections is the porcupine. Four specimens (2.9%) from the NG-A deposit exhibit gnawing, whereas a much greater proportion of 443 (35.3%) of the total specimens from the NG-B deposit exhibit gnawing. If these assemblages are distinct, it is possible this disparity is due to a much greater porcupine presence during the formation of the NG-B assemblage in comparison to NG-A. However, if NG-B formed as a result of the erosion and redeposition of material from NG-A it is more likely that porcupines only had access to scavenge NG-B specimens on the surface of soft sediments after erosion occurred, as NG-A specimens were shielded by a hard, indurate $CaCO_3$ deposit.

Four specimens from the NG-B deposit and a single specimen from the NG-A deposit display measurable trough marks which range from 2.6 to 6.0 mm, consistent with porcupine gnawing marks (Table S4; Fig. 13). Gnawing is restricted to the periphery of the teeth (partly due to the smaller size of the teeth) and bones. The trough marks are specifically located on the enamel-dentine junction on the sides of the teeth and the articular ends of long bones. Only seven teeth (2%) were missing roots in the NG-A assemblage. In contrast, all but 80 (98%) teeth in the NG-B assemblage have a complete or partial absence of roots, and this is likely evidence of the preferential gnawing of tooth roots by porcupines

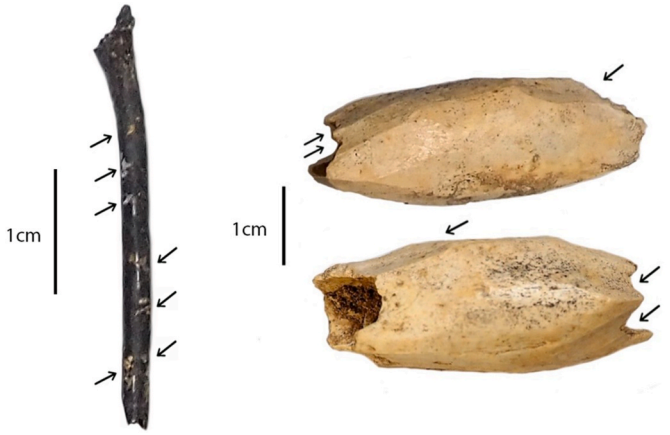

Fig. 13. (Left) Photograph of blackened long bone fragment NG4.16 from the NG-B assemblage exhibiting numerous tiny carnivore tooth pits, scores and punctures; (right) Photograph of visible gnawing marks on bone fragment NG27.10.

(de Vos and Ciochon, 1996). The evidence of porcupine activity is further supported by the presence of this rodent's dental remains in both assemblages.

4.3.5. Depositional setting

Overall, 4% (n = 7) of all specimens from the NG-A assemblage and 24.24% (n = 311) of all specimens from the NG-B assemblage have partial mineral staining or discoloration on their surface area. The staining occurs in dull black and orange-yellow tones, which suggests mineral staining is caused by the presence of manganese oxide and iron (Dupras and Schultz, 2013). The superficial coating is derived from circulating water, dissolved by groundwater in the presence of CO_2 and precipitated by CO_2 loss, oxidation, and evaporation (López-González, 2006). Weathering of bone and tooth specimens was observed in both assemblages. Most specimens in the NG-A assemblage exhibit stage one weathering (98.2%, n = 575) and a small number reach maximally stage three (1.8%, n = 10). In the NG-B assemblage, 59% (n = 256) exhibit stage one weathering, followed by 37.8% (n = 163) in stage three and 3.2% (n = 12) in stage four. Only 3% (n = 16) of the weathered specimens from site NG-B exhibit cortical exfoliation. Abrasion is also evident in both assemblages. In the NG-A assemblage, 17% (n = 31) of remains have first stage abrasion, and no other stages are evident. In the NG-B assemblage, 19% (n = 245) of the NG-B assemblage exhibits first stage abrasion, and a single specimen exhibits third stage abrasion.

4.3.6. Age category

In the NG-A assemblage, ungulates (i.e., suids, cervids, bovids) are best represented by adults (MNI = 7), followed by seniors (MNI = 3) and juveniles (MNI = 1), although it's worth noting the very small sample size. Primates are best represented by adults (MNI = 4), a single senior, and no juveniles. In the NG-B assemblage, ungulates are best represented by adults (MNI = 14), followed by seniors (MNI = 7) and juveniles (MNI = 3). Likewise, primates are best represented by adults (MNI = 10), followed by seniors (MNI = 6) and no juveniles. The most abundant age class evident in the taxonomically identifiable teeth are significantly different between the localities (X^2 (3, N = 389, 104) = 22.13, p = <0.001), with the number of adult teeth proportionally less represented in NG-B, (adults, n = 258; seniors, n = 122; juveniles, n = 9) compared to NG-A (adults, n = 93; seniors, n = 9; juveniles, n = 2). In the NG-A assemblage, carnivores (e.g. felids, viverrids and ursids) are best represented by adults (MNI = 2), with no seniors and juveniles present. In the NG-B assemblage, carnivores are once again best represented by adults (MNI = 9), followed by seniors (MNI = 5) and no juveniles. In the NG-A assemblage, rodents are best represented by adults (MNI = 1) and no juveniles or seniors. In the NG-B assemblage, rodents are best represented by adults (MNI = 3) and seniors (MNI = 3), and no juveniles. Taken together, adults are best represented at Ngalau Gupin, followed by seniors, and very few juveniles. The underrepresentation of juvenile teeth may, however, be due to a greater susceptibility of juvenile bones and teeth to destruction (Lyman, 1994; Munson, 2000; Munson and Gariewicz, 2003). Indeed, all surviving deciduous teeth originate from large animals with thick enamel and dentine such as *Tapirus indicus*, Cervidae, Rhinocerotidae and Elephantidae.

5. Discussion

This study represents the first taxonomic, taphonomic, and chronological study of fossil faunal assemblages from Ngalau Gupin Cave in the Padang Highlands, Sumatra, and one of only several such studies for the entire island. This research acts as an important contribution to elucidating the processes of site formation that determine fossil preservation state in this tropical sub-region. Our taphonomic assessment of the assemblages revealed a complex history of carnivore and porcupine accumulation and post-depositional attrition.

5.1. Comparative study of NG-A and NG-B

The fossils from the NG-B unconsolidated sediments on the cave floor were recovered from directly below the NG-A fossiliferous breccia and there is a remarkable amount of taxonomic overlap between the two deposits. Furthermore, the taxa are similarly represented in terms of abundance, necessitating a consideration of whether these are distinct fossil assemblages, or if NG-B formed because of the erosion and redeposition of material from NG-A (our null hypothesis).

Combined observations of speleology, geology, taphonomy and species presence suggest that the NG-B locus is most likely the result of erosion from the NG-A breccias. The fauna in both sites consists of predominantly modern taxa, with most representatives still living in the area (e.g., *Macaca*, *Pongo*, *Panthera tigris,* and *Elephas*) or elsewhere in Southeast Asia (e.g., *Rhinoceros unicornis* and *Rhinoceros sondaicus*). The sole exception to this is the presence of *Hexaprotodon*, which represents the first time hippos have been recovered from Sumatra.

Both assemblages are comprised mostly of isolated dental remains and heavily fragmented bone specimens. Wolff (1973) suggested that assemblages dominated by isolated teeth and fragmented bone have often undergone hydrodynamic sorting. Despite the evidence for wet conditions, the presence of complete small mammals remains suggests that water flow through the cave was neither regular nor particularly strong. High energy waterflow, combined with the angular limestone clasts that characterise the Ngalau Gupin sediments, is likely to have destroyed fragile small animal remains (e.g. Andrews and Cook, 1990).

Water action, however, is not the only process that can create this bias of isolated dental remains. Prevalently in Southeast Asia, rodents, and in particular porcupines, are renowned accumulators of bones and teeth, and there is evidence for porcupine gnawing, as well as porcupine fossils, at Ngalau Gupin. The degree of transformation in the NG-B assemblage suggests that porcupines are likely to play a significant role in the modification and probably in the accumulation of the assemblage. Prolific gnawing behaviour is related to honing porcupine incisors and may also provide some essential nutrients (Brain, 1981). Porcupine accumulations can be abundant in the vicinity of a carnivore lair and bones can be collected from many different predators to reveal a broad spectrum of plausible prey animals and predators (Brain, 1981; O'Regan et al., 2011).

Adult ungulates and primates are most common in Ngalau Gupin deposits. Size of the prey is correlated with the size of carnivores. Regarding ungulates, this may reflect predation by large carnivores such as tigers. Tigers have a broad diet that includes a variety of ungulates and primates (O'Brien et al., 2003) and they are known to preferentially target adults averaging 91.5 kg (Karanth and Sunquist, 1995). Hominins

are also known to preferentially target adult individuals (e.g. Bar-Oz et al., 2005; Zhang et al., 2009) but a hominin role in the accumulation of bones at Ngalau Gupin can be excluded based on (1) the lack of anthropogenically modified bone and (2) the age of the Ngalau Gupin material, which pre-dates the earliest known hominin presence in Sumatra. However, we acknowledge that due to the elements preserved in this assemblage and the reconstructed taphonomic pathways, anthropogenic modifications and/or tools, if they had been present, would be very unlikely to preserve. There are several potential predators of these species in SE Asia including birds of prey and cats (e.g. Van Schaik and Van Noordwijk, 1985; McGraw and Berger, 2013). Given the scarcity of bone remains and associated bone surface modifications it remains difficult to confidently comment on the likely contributor of the death assemblage leading to the Ngalau Gupin collection; however, the ungulate and primate age profiles are most consistent with the hunting behaviour of a large carnivore.

Small animals like rodents and birds tend to have very different preservational pathways compared to larger animals (Andrews and Cook, 1990). One of the main accumulating agents of small animal remains in cave deposits are raptors (e.g., owls) which deposit dense concentrations of small animal bones at their nesting sites in the form of pellets (Andrews and Cook, 1990; Hawkins et al. 2017, 2018). Perhaps the clearest sign of raptor predation is acid corrosion resulting from gastric acid acting on bones following consumption (Fernández-Jalvo et al., 2016). However, none of the Ngalau Gupin small animal remains exhibit acid corrosion and therefore accumulation by a raptor appears unlikely.

The bones in the Ngalau Gupin collection exhibit fracture patterns consistent with both green and dry fracturing of bone. The green fractures may be the result of carnivore processing, further evident in the small carnivore punctures seen on one of the small mammal specimens. The dry fracturing may have occurred at a later time, and may have been caused by trampling, rock fall, and/or burial. In some karstic sites (like Ma U'Oi in Vietnam; Bacon et al., 2004, 2006), two types of assemblages can be observed: one of only large mammals, and another of only microfauna. This is due to different dynamics of deposition: the assemblage can be a mixture of large mammal fossils and more recent microfauna from the surface. Our observations suggest the very small mammal bones in Ngalau Gupin (i.e. bats) looked fresh and were probably more recent than the other taxa.

Tropical caves are prone to inundation by water and high levels of humidity, making them less-than-ideal places for the long-term preservation of bones (Andrews and Cook, 1985; Fernández-Jalvo et al., 2010; Morley and Goldberg, 2017). The precipitation of manganese oxide on fossil surfaces in both assemblages indicates the cave environment was wet and mildly alkaline, which is supported by the presence of fossil molluscs. In addition, a small number of NG-B fossils exhibit cortical exfoliation, a common indicator that fossils were exposed to repeated cycles of wet-dry conditions. Staining is less common in the NG-A assemblage and this may be because these fossils were protected by the calcium carbonate cement.

Taken together, our data suggests that the mammal remains were initially deposited in the landscape surrounding the cave, perhaps as the result of large carnivore predation. Following this, animal remains were modified in the cave by porcupine gnawing, leaving mostly teeth. The remains were then cemented into the NG-A assemblage forming consolidated breccia. The significant overlap in the faunal representation in both assemblages, as well as evidence for more pronounced staining, damage, and weathering of the specimens from NG-B, suggest that fossils eroded out of NG-A and were redeposited into the unconsolidated NG-B sediments directly below, following a small amount of lateral and vertical movement aided by low energy water flow. Most small animal remains, however, may have been deposited by small carnivores, although positive evidence for this is based on a single specimen and so it is unclear precisely how small mammal remains accumulated.

5.2. Age of Ngalau Gupin

In the first instance, the significant age difference between SUM18-21a from NG-A and SUM18-22a from NG-B (i.e., the two samples providing finite combined US-ESR age estimates), might be used as evidence suggesting that the fossil assemblages from the two loci are not coeval. However, this may also be a calculation artefact due to the very specific features displayed by the teeth. When using the sediment sample SUM18-11 collected from NG-A, the resulting age (SUM18-21b) of about 60 ka becomes very close to those obtained from NG-B. In other words, the apparent age difference is only due to the sediment samples used in the dose rate evaluation. Although sediment samples collected at NG-A and NG-B display very different radioelement concentrations, the overall gamma dose rate that may be derived are virtually the same (465 vs 460 μGy/a). Additionally, although the ESR data do not show any major differences between NG-A and NG-B teeth, the U-series instead seem to indicate slightly different uranium uptakes (See Table 1).

This may well originate from different depositional histories, or simply be the results of a more recent change in the geochemistry of the surrounding environment, as the result of erosion and reworking from NG-A. If reworking can be unambiguously demonstrated, then the ESR age results obtained for NG-B fossils should be taken with extreme caution. By principle, the ESR dose rate reconstruction is based on the assumption that the current sedimentary environment has prevailed throughout the sample's burial history. If not, then it is virtually impossible to properly and accurately evaluate the gamma dose rate associated to the tooth that is being dated. This issue is even more crucial in the present case, where the dose rate from the sediment represents >90% of the total dose rate.

SUM18-21a most likely provides the most reliable chronological constraint for Ngalau Gupin fossil assemblage because (i) it comes from the original breccia deposits of NG-A, which is less likely to have been impacted by sedimentary reworking processes, and (ii) it was the only tooth for which the sediment was directly attached. Dental tissues represent <10% of the total dose rate, which is thus mostly dominated by the component from the sediment. Consequently, sources of uncertainty associated with the external dose rate evaluation may significantly impact the calculated ESR ages. In particular, we have identified two crucial parameters in that regard: (i) the water content and (ii) the vicinity of the limestone wall.

Age calculations were initially performed using the current water content (25 ± 5%) measured in sediment samples SUM18-11 and SUM18-12. However, one may reasonably consider that humidity conditions may have changed over time. Consequently, some sensitivity tests were performed in order to evaluate the impact of the assumed water content on the calculated ESR ages (Fig. 14a). For sample SUM18-21a, increasing the water content (WC) by +5% and 10% would make the age older by +8% and 18%, respectively. The age estimates would increase from ca. 134 ka (25% WC) to ca. 145 ka (30% WC) and ca. 158 ka (35% WC). The latter would still overlap within 2-σ with the initial US-ESR age calculation performed for sample SUM18-21a and considering water content values > 35% seems presently purely speculative. Instead, when using a value of 15%, which approximately corresponds to the value measured in the breccia deposits from the nearby Sumatran site of Lida Ajer (Westaway et al., 2017), the combined US-ESR age result decreases by about 13% and reaches 116 + 10–9 ka.

Initial age calculations were performed assuming that 100% of the gamma dose rate was coming from the breccia. However, field observations suggest that the limestone wall was <30 cm from the tooth, most likely around 15 cm. This may impact the accuracy of the gamma dose rate, as limestone is typically not very radioactive compared to sediment, which may be approximated in first instance as a virtually inert material. Consequently, some age simulations were performed by considering the relative distance to limestone and correcting the gamma dose rate accordingly using Aitken (1985). As expected, the closer to the limestone wall and the older the age gets (Fig. 14b). However, when

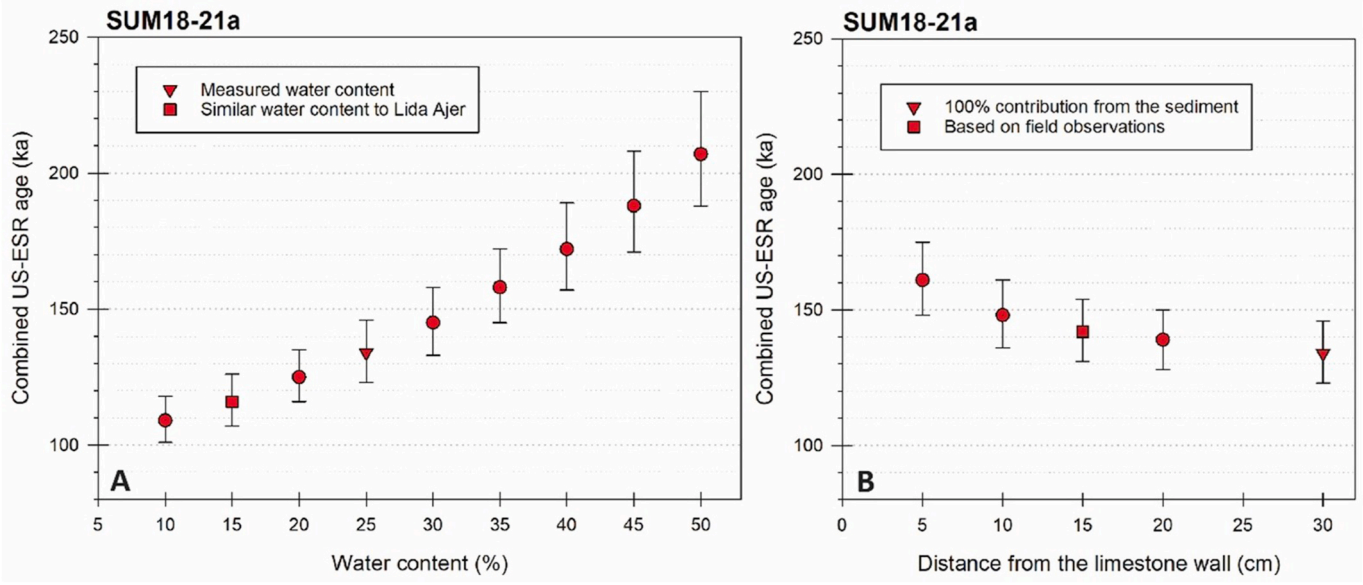

Fig. 14. Age sensitivity tests for tooth SUM18-21a. A: Impact of water content (% wet weight) on calculated combined US-ESR age estimates. The measured water content is 25% (values corresponding to the SUM1821a age calculation displayed in Table 1). The 15% (% wet weight) correspond approximately to the value measured in Lida Ajer (Westaway et al., 2017). B: impact of the distance from limestone on the calculated combined US-ESR age estimates. The 30-cm distance corresponds to the calculation displayed in Table 1 for SUM1821a.

considering the 15 cm distance, the combined US-ESR age gets slightly older by only about 8 ka (+6%) but remains nevertheless within error. Although we acknowledge an inherent uncertainty around the gamma dose rate, given the heterogeneity of the deposits and the absence of *in situ* measurements, these calculations illustrate the limited impact of the limestone wall vicinity on the calculated ages.

In summary, combined US-ESR dating of SUM18-21 sample indicate that the age of fossil assemblage at Ngalau Gupin lies somewhere between ~160 ka and ~115 ka, depending on the long-term water content value selected for the dose rate evaluation.

5.3. Implications of Ngalau Gupin study

Our results correlate the Ngalau Gupin fauna with either the second half of the MIS 5 or the beginning of MIS 6. The faunas from this site are essentially modern, and most likely represents a rainforest environment much like found locally today. Nevertheless, the site records several important extirpations of large bodied taxa. This study indicates that the Indian and Javan rhinos *Rhinoceros unicornis* and *Rhinoceros sondaicus* and the proboscis monkey *Nasalis* were present in the Pleistocene of the Padang Highlands. It also provides the first evidence of *Hexaprotodon* from Sumatra. A detailed and quantitative analysis of the palaeoenvironments represented by the Ngalau Gupin assemblage is needed to provide insights into plausible extinction mechanisms operating on the island; however, it is interesting to note that neither *Hexaprotodon, Nasalis,* nor *Rhinoceros unicornis* have been recovered from the younger site of Lida Ajer, which incidentally hosts the earliest record of *Homo sapiens* on the island (Westaway et al., 2017).

Within the wider context of the Southeast Asian faunal assemblage, Ngalau Gupin shares similar faunal elements with other near-contemporaneous sites such as Punung in Java (Westaway et al., 2007), Tham Wiman Nakin in Thailand (Tougard, 1994, 1996, 1998; Suraprasit et al. 2016, 2020), Tam Hang South in Laos (Bacon et al., 2015), and Nam Lot and Coc Muoi (Bacon et al., 2018) in Vietnam. Lowered sea levels during the latter part of MIS 6 and into MIS 5 may have promoted connections, faunal migrations, and faunal turnovers between these different regions (Long et al., 1996).

When compared to the site of Ngandong in Java, Ngalau Gupin differs considerably in terms of the fauna present and environments that were likely present. While several modern taxa are found in both Ngalau Gupin and Ngandong, including *Macaca fascicularis*, *Panthera tigris*, *Tapirus indicus* and *Rhinoceros sondaicus*, Ngandong nevertheless contains several extinct species that are not seen in Ngalau Gupin including *Stegodon trigonocephalus*, *Bubalus palaeokerabau*, *Sus macrognathus*, and *Homo erectus* (Rizal et al., 2020). The traditional view has been that modern rainforests appeared in Java, and by inference Sumatra, around the time of the deposition of Punung, and following on from the open woodlands associated with Ngandong (de Vos et al., 1983; Westaway et al., 2007). The Ngalau Gupin record, however, indicates a largely modern rainforest fauna existed in Sumatra prior to Ngandong. This suggests that rainforest persisted at least at the periphery of Sundaland (Ngalua Gupin, Punung) during periods when open woodland environments dominated the interior of the exposed Sunda shelf.

6. Conclusion

Ngalau Gupin represents a significant new palaeontological locality in Southeast Asia. Excavation of the NG-A and NG-B loci within the cave produced a rich, diverse suite of faunal remains, and produced the first evidence of *Hexaprotodon* in the Sumatran fossil record. Our results indicate that the NG-B assemblage was redeposited after being eroded from the NG-A breccias. Direct dating of the faunal assemblages suggests a late MIS 6 or early MIS 5 age. Additionally, our results provide an important case study on the limitations of dating in the complex cave environments, a subject that has important implications for interpreting fossil records from the region (e.g. Westaway et al., 2007; Bacon et al., 2008; O'Connor et al., 2010, 2017; Louys et al., 2017). The taphonomic data indicate that the Ngalau Gupin collection is composed of an assemblage with at least two different taphonomic pathways. The medium-to large sized mammal dental remains appear to represent a prime-dominated death assemblage accumulated by large carnivores and subsequently gathered by porcupines, whereas the small mammal post-cranial material may have been accumulated by smaller carnivores. Our analysis of the taphonomic and depositional history of Ngalau Gupin fossil remains, within a detailed speleological and geochronological framework, provides important first insights into a diverse Pleistocene megafauna community from before human arrival in Sumatra.

Author contributions

H.E.S contributed to the fieldwork, data acquisition, analysis and interpretation, and primary authorship of the manuscript. G.J.P contributed to fieldwork, dating, data acquisition, and authorship. M.D. contributed to the dating of fossil specimens and fossil-bearing sediments and authorship. K.W contributed to the dating of fossil-bearing sediments and authorship. Y.R, J.Z, M.R.P, A, A.T contributed to fieldwork and collection and curation of materials. M.S contributed to cataloguing of the specimens and authorship. J.L contributed to the conception of the research, fieldwork, data acquisition and interpretation, and the authorship of this article. All authors contributed to the development of the manuscript.

Data availability

The data used to support the findings of this study are available with the paper and its supplementary files.

Declaration of competing interest

The authors declare that they have no known competing financial interests or personal relationships that could have appeared to influence the work reported in this paper.

Acknowledgements

We thank the students and staff at Institut Teknologi Bandung for their assistance during fieldwork and their invaluable contributions to this project. We appreciate the support of Dr Hilary Ketchum and Ms Eileen Westwig for access to comparative osteological materials in the Oxford Museum of Natural History in London. M.D. is grateful to María Jesús Alonso Escarza, Javier Iglesias Cibanal, David Martínez Asturias, & Leticia Miguens Rodríguez, CENIEH, for technical support throughout the dating analytical procedure. This study was funded by Australian Research Council (ARC) Future Fellowship (FF) FT160100450 granted to J.L. Aspects of the combined U-series/ESR analyses have been funded by the Australian Research Council Future Fellowship Grant FT150100215 and the Spanish Ramón y Cajal Fellowship RYC2018-025221-I granted to M.D. H.S's Postgraduate & Research Scholarships were provided by the Australian Research Centre for Human Evolution, Griffith University, Brisbane. We thank our reviewers for their valuable input. We thank Ms Christina Engl for support in illustration software and Dr Douglas Kerlin for statistical support.

Appendix A. Supplementary data

Supplementary data to this article can be found online at https://doi.org/10.1016/j.quaint.2021.05.005.

References

Aitken, M.J., Clark, P.A., Gaffney, C.F., Løvborg, L., 1985. Beta and gamma gradients, 1982 Nucl. Tracks Radiat. Meas. 10 (4–6), 647–653.
Andrés, M., Gidna, A.O., Yravedra, J., Domínguez-Rodrigo, M., 2012. A study of dimensional differences of tooth marks (pits and scores) on bones modified by small and large carnivores. Archaeological and Anthropological Sciences 4, 209–219.
Andrews, P., Cook, J., 1985. Natural modifications to bones in a temperate setting. Man 20 (4), 675–691.
Andrews, P., Cook, J., 1990. Owls, Caves and Fossils: Predation, Preservation and Accumulation of Small Mammal Bones in Caves, with an Analysis of the Pleistocene Cave Faunas from Westbury-sub-Mendip. University of Chicago Press, Somerset, UK.
Bacon, A.-M., Long, V.T., 2001. The first discovery of a complete skeleton of a fossil orang-utan in a cave of the Hoa Binh Province, Vietnam. J. Hum. Evol. 41 (3), 227–241.
Bacon, A.M., Demeter, F., Schuster, M., Long, V.T., Thuy, N.K., Antoine, P.O., Sen, S., Nga, H.H., Huong, N.M., 2004. The Pleistocene Ma U'Oi cave, northern Vietnam: palaeontology, sedimentology and palaeoenvironments. Geobios 37, 305–314.
Bacon, A.-M., Demeter, F., Rousse, S., Long, V.T., Duringer, P., Antoine, P.-O., Thuy, N. K., Mai, B.T., Huong, N.T.M., Dodo, Y., 2006. New palaeontological assemblage, sedimentological and chronological data from the Pleistocene Ma U'Oi cave (northern Vietnam). Palaeogeogr. Palaeoclimatol. Palaeoecol. 230, 280–298.
Bacon, A.M., Demeter, F., Duringer, P., Helm, C., Bano, M., Long, V.T., Thuy, N.T.K., Antoine, P.-O., Mai, B.T., Huong, N.T.M., Dodo, Y., 2008. The Late Pleistocene Duoi U'Oi cave in northern Vietnam: palaeontology, sedimentology, taphonomy and palaeoenvironments. Quat. Sci. Rev. 27, 1627–1654.
Bacon, A.M., Westaway, K., Antoine, P.O., Duringer, P., Blin, A., Demeter, F., Ponche, J.-L., Zhao, J.-X., Barnes, L.M., Sayavonkhamdy, T., Thuy, N.T.L., Long, V.T., Edoumba, E., Shackleford, L., 2015. Late Pleistocene mammalian assemblages of Southeast Asia: new dating, mortality profiles and evolution of the predator-prey relationships in an environmental context. Palaeogeogr. Palaeoclimatol. Palaeoecol. 422, 101–127.
Bacon, A.-M., Antoine, P.-O., Huong, N.T.M., Westaway, K., Tuan, N.A., Duringer, P., Zha, J.-X., Ponch, J.-L., Dung, S.C., Nghia, T.H., 2018. A rhinocerotid-dominated megafauna at the MIS6-5 transition: the late middle Pleistocene Coc Muoi assemblage, lang son province, Vietnam. Quat. Sci. Rev. 186, 123–141.
Badgley, C., 1986. Counting individuals in mammalian fossil assemblages from fluvial environments. Palaios 3, 328–338.
Badoux, D.M., 1959. Fossil Mammals from Two Fissure Deposits at Punung, Java: with Some Remarks on Migration and Evolution of Mammals during the Quaternary in South East Asia. Kemink en Zoon N.V, Utrecht, Netherlands.
Baludikay, B.K., Storme, J.-Y., François, C., Baudet, D., Javaux, E.J., 2016. A diverse and exquisitely preserved organic-walled microfossil assemblage from the Meso–Neoproterozoic Mbuji-Mayi Supergroup (Democratic Republic of Congo) and implications for Proterozoic biostratigraphy. Precambrian Res. 281, 166–184.
Bar-Oz, G., Weinstein-Evron, M., Livne, P., Zaidner, Y., O'Connor, T., 2005. Fragments of information: preliminary taphonomic results from the middle palaeolithic breccia layers of misliya cave, mount carmel, Israel. In: Biosphere to Lithosphere: New Studies in Vertebrate Taphonomy. Oxbow Press, Oxford, pp. 128–136.
Barker, G., Barton, H., Bird, M., Daly, P., Datan, I., Dykes, A., Farr, L., Gilbertson, D., Harrisson, B., Hunt, C., Higham, T., 2007. The 'human revolution' in lowland tropical Southeast Asia: the antiquity and behavior of anatomically modern humans at Niah Cave (Sarawak, Borneo). J. Hum. Evol. 52, 243–261.
Behrensmeyer, A.K., 1978. Taphonomic and ecologic information from bone weathering. Paleobiology 4, 150–162.
Behrensmeyer, A.K., Hill, A.P., 1988. Fossils in the Making: Vertebrate Taphonomy and Paleoecology, vol. 69. University of Chicago Press.
Berkovitz, B., Shellis, P., 2018. The Teeth of Mammalian Vertebrates. Academic Press, London.
Boisserie, J.-R., White, T.D., 2004. A new species of pliocene hippopotamidae from the middle awash, Ethiopia. J. Vertebr. Paleontol. 24, 464–473.
Bowen, W.H., Koch, G., 1970. Determination of age in monkeys (*Macaca irus*) on the basis of dental development. Lab. Anim 4, 113–123.
Brain, C.K., 1981. The Hunters or the Hunted? an Introduction to African Cave Taphonomy. University Chicago Press, Chicago.
Brünnich, M.T., 1772. Zoologiæ fundamenta prælectionibus academicis accomodata. Grunde i Dyrelæren 1–253.
Bunn, H.T., 1982. Meat-eating and Human Evolution: Studies on the Diet and Subsistence Patterns of Plio-Pleistocene Hominids in East Africa. University of Wisconsin, Madison, Unpublished PhD thesis.
Bunn, J.M., Ungar, P.S., 2009. Dental topography and diets of four old world monkey species. Am. J. Primatol. 71, 466–477.
Bunn, H.T., Kroll, E.M., Ambrose, S.H., Behrensmeyer, A.K., Binford, L.R., Blumenschine, R.J., Klein, R.G., McHenry, H.M., O'Brien, C.J., Wymer, J.J., 1986. Systematic butchery by Plio/Pleistocene hominids at Olduvai Gorge, Tanzania [and comments and reply]. Curr. Anthropol. 27, 431–452.
Chaplin, R.E., 1971. The Study of Animal Bones from Archaeological Sites. Seminar, London.
Chapman, N.G., Brown, W., Rothery, P., 2005. Assessing the age of Reeves' muntjac (Muntiacus reevesi) by scoring wear of the mandibular molars. J. Zool. 267, 233–247.
Cheng, H., Edwards, R.L., Hoff, J., Gallup, C.D., Richards, D.A., Asmerom, Y., 2000. The half-lives of uranium-234 and thorium-230. Chem. Geol. 169, 17–33.
Christiansen, P., 2008. Feeding ecology and morphology of the upper canines in bears (Carnivora: Ursidae). J. Morphol. 269, 896–908.
Clark, T.R., Roff, G., Zhao, J.X., Feng, Y.X., Done, T.J., Pandolfi, J.M., 2014. Testing the precision and accuracy of the U-Th chronometer for dating coral mortality events in the last 100 years. Quat. Geochronol. 23, 35–45.
Colbert, E.H., 1935. Siwalik mammals in the American Museum of Natural History. Trans. Am. Phil. Soc. 26. https://doi.org/10.2307/1005467.
Coryndon, S., 1970. The extent of variations in fossil Hippopo tamus from Africa. Symp. Zool. Soc 135–147.
Coryndon, S.C., 1977. The taxonomy and nomenclature of the Hippopotamidae (Mammalia, Artiodactyla) and a description of two new fossil species. Proc. Koninklijke Nederl. Akademie Wetenschappen B 80, 61–88.
Cucchi, T., Fujita, M., Dobney, K., 2009. New insights into pig taxonomy, domestication and human dispersal in Island South East Asia: molar shape analysis of *Sus* remains from Niah Caves, Sarawak. Int. J. Osteoarchaeol. 19, 508–530.
De Marco, A., Cozzolino, R., Thierry, B., 2018. Prolonged transport and cannibalism of mummified infant remains by a Tonkean macaque mother. Primates 59, 55–59.
de Vos, J., 1983. The Pongo faunas from Java and Sumatra and their significance for biostratigraphical and paleo-ecological interpretations. Proc. Koninklijke Nederl. Akademie Wetenschappen 86, 417–425.
Denys, C., 2002. Taphonomy and experimentation. Archaeometry 44, 469–484.
Desmarest, A.G., 1819. Nouveau Dictionnaire D'histoire Naturelle. Chez Deterville, Paris.

Dharma, B., 1992. Indonesian Shells II (Siput Dan Kerang Indonesia II). Wiesbaden, pp. 1–158.
Dharma, B., 2005. Recent and Fossil Indonesian Shells. Hackenheim, pp. 1–424.
Dharma, B., Grego, J., Szekeres, M., 2009. Three new species of clausiliids (Gastropoda, pulmonata, Clausiliidae) from Indonesia. Basteria 73, 85–90.
Dong, W., Chen, S.K., 2015. An extraordinary pattern of ruminant molars and associated cervids from the Pleistocene of Wushan. Central China 53, 207–218.
Drawhorn, G.M., 1994. The Systematics and Paleodemography of Fossil Orangutans (Genus Pongo). University of California, Davis.
Dubois, E., 1891. Voorloopig bericht omtrent het onderzoek naar de Pleistocene en tertiaire Vertebraten-Fauna van Sumatra en Java, gedurende het jaar 1890. Natuurkundig Tijdschrift voor Nederlandsch Indie 51, 93–100.
Dupras, T.L., Schultz, J.J., 2013. Taphonomic bone staining and color changes in forensic contexts. In: Pokines, J.T., Symes, S.A. (Eds.), Manual of Forensic Taphonomy. CRC Press, Boca Raton, Florida, pp. 315–340.
Duringer, P., Bacon, A.M., Sayavongkhamdy, T., Nguyen, T.K.T., 2012. Karst development, breccias history, and mammalian assemblages in Southeast Asia: a brief review. Comptes Rendus Palevol 11, 133–157.
Duval, M., Grün, R., 2016. Are published ESR dose assessments on fossil tooth enamel reliable? Quat. Geochronol. 31, 19–27.
Duval, M., Martín-Francés, L., 2017. Quantifying the impact of μCT-scanning of human fossil teeth on ESR age results. Am. J. Phys. Anthropol. 163, 205–212.
Duval, M., Westaway, K., Zaim, J., Rizal, Y., Aswan, Puspaningrum, M., Trihascaryo, A., Smith, H.E., Drawhorn, G.M, Price, G.J and Louys, J., (Manuscript in preparation) New Chronological Constraints for the Late Pleistocene Fossil Assemblage and Associated Breccia from Ngalau Sampit, (Sumatra).
Falconer, H., Cautley, P.T., 1836. Note on the fossil Hippopotamus of the Sivalik hills. Asiatic Research 19, 39–53.
Farooq, U., Khan, M.A., Akhtar, M., Khan, A.M., 2008. Lower dentition of *Dorcatherium majus* (Tragulidae, Mammalia) in the lower and middle siwaliks (miocene) of Pakistan. Turk. J. Zool. 32, 91–98.
Fernández-Jalvo, Y., Andrews, P., Pesquero, D., Smith, C., Marin-Monfort, D., Sanchez, B., Geigl, E.-M., Alonso, A., 2010. Early bone diagenesis in temperate environments: Part I: surface features and histology. Palaeogeogr. Palaeoclimatol. Palaeoecol. 288, 62–81.
Fernández-Jalvo, Y., Andrews, P., Denys, C., Sesé, C., Stoetzel, E., Marin-Monfort, D., Pesquero, D., 2016. Taphonomy for taxonomists: implications of predation in small mammal studies. Quat. Sci. Rev. 139, 138–157.
Filoux, A., Wattanapituksakul, 2019. The Late Pleistocene Orangutan from Tham Prakai Phet: New Discoveries, vol. 105. Annales de Paléontologie.
Filoux, A., Wattanapituksakul, A., Lespes, C., Thongcharoenchaikit, C., 2015. A Pleistocene mammal assemblage containing *ailuropoda* and *Pongo* from Tham prakai phet cave, chaiyaphum province, Thailand. Geobios 48, 341–349.
Florin, S.A., Fairbairn, A.S., Nango, M., Djandjomerr, D., Marwick, B., Fullagar, R., Smith, M., Wallis, L.A., Clarkson, C., 2020. The first Australian plant foods at Madjedbebe, 65,000–53,000 years ago. Nat. Commun. 11, 1–8.
Francis, C., 2017. Mammals of South-East Asia. Bloomsbury Publishing.
Frisch, J.E., 1967. The gibbons of the Malay peninsula and of Sumatra. Primates 8, 297–310.
Gregory, W.K., Hellman, M., 1939. On the evolution and major classification of the civets (Viverridae) and allied fossils and recent Carnivora: a phylogenetic study of the skull and dentition. Proc. Am. Phil. Soc. 81, 309–392.
Grohé, C., Chaimanee, Y., De Bonis, L., Yamee, C., Blondel, C., Jaeger, J.J., 2010. New data on Mustelidae (Carnivora) from Southeast Asia: *Siamogale thailandica*, a peculiar otter-like mustelid from the late middle miocene mae moh basin, northern Thailand. Naturwissenschaften 97, 1003–1015.
Groves, C.P., 1983. Phylogeny of the living species of rhinoceros. J. Zool. Syst. Evol. Res. 21, 293–313.
Grün, R., 2000a. Methods of dose determination using ESR spectra of tooth enamel. Radiat. Meas. 32, 767–772.
Grün, R., 2000b. An alternative model for open system U-series/ESR age calculations: (closed system U-series)-ESR, CSUS-ESR. Ancient TL 18, 1–4.
Grün, R., 2009. The DATA program for the calculation of ESR age estimates on tooth enamel. Quat. Geochronol. 4, 231–232.
Grün, R., Brumby, S., 1994. The assessment of errors in past radiation doses extrapolated from ESR/TL dose-response data. Radiat. Meas. 23, 307–315.
Grün, R., Katzenberger-Apel, O., 1994. An alpha irradiator for ESR dating Ancient. TL 12, 35–38.
Grün, R., et al., 1988. ESR dating of tooth enamel: coupled correction for U-uptake and U-series disequilibrium. Int. J. Radiat. Appl. Instrum. Nucl. Tracks Radiat. Meas. 14, 237–241.
Guérin, C., 1980. Les rhinocéros (Mammalia, Perissodactyla) du Miocène terminal au Pléistocène supérieur en Europe occidentale. In: Comparaison avec les espèces actuelles, vol. 79. Documents du Laboratoire de Géologie de la Faculté des Sciences de Lyon, pp. 1–1182.
Guérin, G., et al., 2011. Dose-rate conversion factors: update. Ancient TL 29, 5–8.
Hammer, Ø., Harper, D.A., Ryan, P.D., 2001. PAST: paleontological statistics software package for education and data analysis. Palaeontol. Electron. 4, 9.
Harrison, T., Jin, C., Zhang, W., Wang, Y., Zhu, M., et al., 2014. Fossil Pongo from the Early Pleistocene Gigantopithecus fauna of Chongzuo, Guangxi, southern China. Quat. Int. 354.
Hawkins, S., O'Connor, S., Maloney, T.R., Litster, M., Kealy, S., Fenner, J.N., Aplin, K., Boulanger, C., Brockwell, S., Willan, R., Piotto, E., Louys, J., 2017. Oldest human occupation of Wallacea at Laili Cave, Timor-Leste, shows broad-spectrum foraging responses to late Pleistocene environments. Quat. Sci. Rev. 171, 58–72.
Hawkins, S., Samper Carro, S.C., Louys, J., Aplin, K., O'Connor, S., Mahirta, 2018. Human palaeoecological interactions and owl roosting at tron bon lei, alor island, eastern Indonesia. J. I. Coast Archaeol. 13, 371–387.
Haynes, G., 1983. A guide for differentiating mammalian carnivore taxa responsible for gnaw damage to herbivore limb bones. Paleobiology 9, 164–172.
Hillson, S., 2005. Teeth. Cambridge University Press.
Hillson, S., 2016. Mammal Bones and Teeth: an Introductory Guide to Methods of Identification. Routledge.
Hilton, J., Wang, S.-J., Galtier, J., Li, C.-S., 2001. An Early Permian plant assemblage from the Taiyuan Formation of northern China with compression/impression and permineralized preservation. Rev. Palaeobot. Palynol. 114, 175–189.
Hooijer, D.A., 1947a. Pleistocene remains of *Panthera tigris* (Linnaeus) subspecies from Wanhsien, Szechwan, China, compared with fossil and recent tigers from other localities. Am. Mus. Novit. 1346.
Hooijer, D.A., 1947b. On fossil and prehistoric remains of *Tapirus* from Java, Sumatra and China. Zool. Meded. 27, 253–299.
Hooijer, D.A., 1948. Prehistoric teeth of man and of the orang-utan from Central Sumatra, with notes on the fossil orang-utan from Java and Southern China. Zool. Meded. 29, 175–301.
Hooijer, D.A., 1950. The Fossil Hippopotamidae of Asia, with Notes on the Recent Species. EJ Brill.
Hooijer, D.A., 1958. Fossil Bovidae from the Malay archipelago and the Punjab. Zool. Verhandel. 38, 1–110.
Hooijer, D.A., 1960. Quaternary gibbons from the Malay archipelago. Zool. Verhandel. 46, 1–42.
Joordens, J.C., Wesselingh, F.P., de Vos, J., Vonhof, H.B., Kroon, D., 2009. Relevance of aquatic environments for hominins: a case study from Trinil (Java, Indonesia). J. Hum. Evol. 57, 656–671.
Joordens, J.C., D'errico, F., Wesselingh, F.P., Munro, S., de Vos, J., Wallinga, J., Ankjaergaard, C., Reimann, T., Wubrans, J.R., Kuipe, K.F., 2015. Homo erectus at Trinil on Java used shells for tool production and engraving. Nature 518, 228–231.
Kaiser, G.W., 2010. The Inner Bird: Anatomy and Evolution. UBC Press.
Karanth, K.U., Sunquist, M.E., 1995. Prey selection by tiger, leopard and dhole in tropical forests. J. Anim. Ecol. 64, 439–450.
Kay, R.F., 1975. The functional adaptations of primate molar teeth. Am. J. Phys. Anthropol. 43, 195–215.
Kay, R.F., 1978. Molar structure and diet in extant Cercopithecidae. In: Butler, P.M., Joysey, K.A. (Eds.), Development, Function and Evolution of Teeth. Academic Press, New York, pp. 309–339.
Kay, R.F., Cant, J.G., 1988. Age assessment using cementum annulus counts and tooth wear in a free-ranging population *of Macaca mulatta*. Am. J. Primatol. 15, 1–15.
King, D., Green, B., 1999. Goannas: the Biology of Varanid Lizards. UNSW Press.
Klippel, W.E., Synstelien, J.A., 2007. Rodents as taphonomic agents: bone gnawing by brown rats and gray squirrels. J. Forensic Sci. 52, 765–773.
Laurie, W.A., Lang, E.M., Groves, C.P., 1983. Rhinoceros unicornis. Mamm. Species 211, 1.
LeRoy, D.O., Levinson, S.A., 1974. A deep-water Pleistocene microfossil assemblage from a well in the northern Gulf of Mexico. Micropaleontology 20, 1–36.
Leslie Jr., D.M., 2011. *Rusa unicolor* (Artiodactyla: Cervidae). Mamm. Species 43 (871), 1–30.
Long, V.T., De Vos, J., Ciochon, R.S., 1996. A fossil mammal fauna of Vietnam (Lang Trang caves), compared with fossil and recent mammal faunas of southeast Asia: their geographical implications. Bulletin of the Indo-Pacific Prehistory Association 14, 101–109.
Loosjes, F.E., 1953. Monograph of the indo-Australian Clausiliidae. Beaufortia 31, 1–226.
López-González, F., Grandal-d'Anglade, A., Vidal-Romaní, J.R., 2006. Deciphering bone depositional sequences in caves through the study of manganese coatings. J. Archaeol. Sci. 33, 707–717.
Louys, J., 2008. Quaternary extinctions in Southeast Asia. In: Elewa, A.M.T. (Ed.), Mass Extinction. Springer, Berlin, Heidelberg, pp. 159–189.
Louys, J., Meijaard, E., 2010. Palaeoecology of Southeast Asian megafauna-bearing sites from the Pleistocene and a review of environmental changes in the region. J. Biogeogr. 37, 1432–1449.
Louys, J., Roberts, P., 2020. Environmental drivers of megafauna and hominin extinction in Southeast Asia. Nature 586 (7829), 402–406.
Louys, J., Curnoe, D., Tong, H., 2007. Characteristics of Pleistocene megafauna extinctions in Southeast Asia. Palaeogeogr. Palaeoclimatol. Palaeoecol. 243, 152–173.
Louys, J., Kealy, S., O'Connor, S., Price, G.J., Hawkins, S., Aplin, K., Rizal, Y., Zaim, J., Mahirta, Tanudirjo, D.A., Santoso, W.D., Hidayah, A.R., Trihascaryo, A., Wood, R., Bevitt, J., Clark, T., 2017. Differential preservation of vertebrates in Southeast Asian caves. Int. J. Speleol. 46, 379–408.
Ludwig, K.R., 2003. User's Manual for Isoplot/Ex Version 3.0: A Geochronological Toolkit for Microsoft Excel. Berkeley Geochronology Centre, Berkeley.
Lydekker, R., 1884. Indian Tertiary and Post-tertiary Vertebrata: Additional Siwalik Perissodactyla and Proboscidea. Office of Superintendent of Government Printing.
Lyman, R.L., 2008. Quantitative Paleozoology. Cambridge University Press, Cambridge.
Lyman, R.L., Lyman, C., 1994. Vertebrate Taphonomy. Cambridge University Press.
Maffei, L., 2003. The age structure of tapirs (*Tapirus terrestris*) in the Chaco. Tapir Conservation 12, 18–19.
Maglio, V.J., 1973. Origin and evolution of the Elephantidae. Transactions of the American Philosophical Society of Philadelphia, New Series 63, 1–149.
Marsh, R.E., 1999. Beta-gradient Isochrons Using Electron Paramagnetic Resonance: towards a New Dating Method in Archaeology. MSc Thesis, McMaster University.
Mazak, V., 1981. Panthera tigris. Mamm. Species 152, 1–8.

Mcgraw, W.S., Berger, L.R., 2013. Raptors and primate evolution. Evol. Anthropol. Issues News Rev. 22, 280–293.
Mennecart, B., de Perthuis, A., Rössner, G.E., Guzmán, J.A., de Perthuis, A., Costeur, L., 2018. The first French tragulid skull (Mammalia, ruminantia, Tragulidae) and associated tragulid remains from the middle miocene of contres (Loir-et-Cher, France). Comptes Rendus Palevol 17, 189–200.
Mijares, A.S., Detroit, F., Piper, P., Grun, R., Bellwood, P., Aubert, M., Champion, G., Cuevas, N., De Leon, A., Dizon, E., 2010. New evidence for a 67,000-year-old human presence at callao cave, luzon, Philippines. J. Hum. Evol. 59, 123–132.
Monchot, H., Fernandez, P., Gaillard, J.M., 2012. Paleodemographic analysis of a fossil porcupine (*Hystrix refossa* gervais, 1852) population from the upper Pleistocene site of geula cave (mount carmel, Israel). J. Archaeol. Sci. 39, 3027–3038.
Morley, M.W., Goldberg, P., 2017. Geoarchaeological research in the humid tropics: a global perspective. J. Archaeol. Sci. 77, 1–9.
Morley, M.W., Goldeberg, P., Sutikna, T., Tocheri, M.W., Prinsloo, L.C., Saptomo, E.W., Wasisto, S., Roberts, R.G., 2017. Initial micromorphological results from Liang Bua, Flores (Indonesia): site formation processes and hominin activities at the type locality of Homo floresiensis. J. Archaeol. Sci. 77, 125–142.
Munson, P.J., 2000. Age-correlated differential destruction of bones and its effect on archaeological mortality profiles of domestic sheep and goats. J. Archaeol. Sci. 27, 391–407.
Munson, P.J., Garniewicz, R.C., 2003. Age-mediated survivorship of ungulate mandibles and teeth in canid-ravaged faunal assemblages. J. Archaeol. Sci. 30, 405–416.
Nater, A., Mattle-Greminger, M.P., Nurcahyo, A., Nowak, M.G., De Manuel, M., Desai, T., Groves, C., Pybus, M., Sonay, T.B., Roos, C., Lameira, A.R., 2017. Morphometric, behavioral, and genomic evidence for a new orangutan species. Curr. Biol. 27, 3487–3498.
O'Brien, T.G., Kinnaird, M.F., Wibisono, H.T., 2003. Crouching tigers, hidden prey: Sumatran tiger and prey populations in a tropical forest landscape. Anim. Conserv. 6, 131–139.
O'Regan, H., Kuman, K., Clarke, J.R., 2011. The likely accumulators of bones: five cape porcupine den assembalges and the role of porcupines in the post-Member 6 infill at Sterkfontein, South Africa. Journal of Taphonomy 9, 69–87.
Olsen, S.L., Shipman, P., 1988. Surface modification on bone: trampling versus butchery. J. Archaeol. Sci. 15, 535–553.
O'Connor, S., Barham, A., Spriggs, M., Veth, P., Aplin, K., St Pierre, E., 2010. Cave archaeology and sampling issues in the tropics: a case study from Lene Hara Cave, a 42,000 year old occupation site in East Timor, Island Southeast Asia. Aust. Archaeol. 71, 29–40.
O'Connor, S., Barham, A., Aplin, K., Maloney, T., 2017. Cave stratigraphies and cave breccias: implications for sediment accumulation and removal models and interpreting the record of human occupation. J. Archaeol. Sci. 77, 143–159.
Panyutina, A.A., Kuznetsov, A.N., Korzun, L.P., 2013. Kinematics of chiropteran shoulder girdle in flight. Anat. Rec. 296, 382–394.
Peigné, S., Chaimanee, Y., Yamee, C., Srisuk, P., Marandat, B., Jaeger, J.J., 2006. A new member of the mustelida (Mammalia: Carnivora) from the paleogene of southern Asia. J. Vertebr. Paleontol. 26, 788–793.
Pike, A.W.G., Hedges, R.E.M., Van Calsteren, P., 2002. U-series dating of bone using the diffusion-adsorption model. Geochem. Cosmochim. Acta 66, 4273–4286.
Pokines, J.T., Sussman, R., Gough, M., Ralston, C., McLeod, E., Brun, K., Kearns, A., Moore, T.L., 2017. Taphonomic analysis of Rodentia and Lagomorpha bone gnawing based upon incisor size. J. Forensic Sci. 62, 50–66.
Popowics, T.E., 2003. Postcanine dental form in the Mustelidae and Viverridae (Carnivora: Mammalia). J. Morphol. 256, 322–341.
Post, L., 2005. In: Post, L. (Ed.), The Bird Building Book: A Manual for Preparing Bird Skeletons with a Bone Identification Guide. Homer, Alaska.
Price, G.J., Feng, Y.X., Zhao, J.X., Webb, G.E., 2013. Direct U–Th dating of vertebrate fossils with minimum sampling destruction and application to museum specimens. Quat. Geochronol. 18, 1–8.
Rizal, Y., Westaway, K.E., Zaim, Y., van den Bergh, G.D., Bettis, E.A., Morwood, M.J., Huffman, O.F., Grün, R., Joannes-Boyau, R., Bailey, R.M., Westaway, M.C., 2020. Last appearance of *Homo erectus* at Ngandong, Java, 117,000–108,000 years ago. Nature 577, 381–385.
Rolett, B.V., Chiu, M.Y., 1994. Age estimation of prehistoric pigs (*Sus scrofa*) by molar eruption and attrition. J. Archaeol. Sci. 21, 377–386.
Rössner, G.E., 2007. Family Tragulidae. In: Prothero, D.R., Foss, S.E. (Eds.), The Evolution of Artiodactyls. John Hopkins University Press, pp. 213–220.
Schlosser-Sturm, E., Schliemann, H., 1995. Morphology and function of the shoulder joint of bats (Mammalia: Chiroptera). J. Zool. Syst. Evol. Res. 33, 88–98.
Schwartz, J.H., Cuong, N.L., Kha, L.T., Tattersall, I., 1994. A diverse hominoid fauna from the late middle Pleistocene breccia cave of Tham khuyen. Socialist Republic of Vietnam. Anthropological papers of the AMNH (73).
Shao, Q., Bahain, J.-J., Falguères, C., Dolo, J.-M., Garcia, T., 2012. A new U-uptake model for combined ESR/U-series dating of tooth enamel. Quat. Geochronol. 10, 406–411.
Shao, Q., Bahain, J.J., Dolo, J.M., Falguères, C., 2014. Monte Carlo approach to calculate US-ESR age and age uncertainty for tooth enamel. Quat. Geochronol. 22, 99–106.
Shipman, P., 1977. Paleoecology, Taphonomic History and Population Dynamics of the Vertebrate Assemblage from the Middle Miocene of Fort Ternan, Kenya. Unpublished Ph. D. thesis. New York University.
Smith, H.E., Morley, M., Louys, J., 2020. Taphonomic analyses of cave breccia in Southeast Asia: a review and future directions. Open Quat. (6), 1.
Stains, H.J., 1983. Calcanea of members of the Viverridae. Bull. South Calif. Acad. Sci. 82, 17–38.
Sten, S., 2004. Bovine teeth in age assessment, from medieval cattle to Belgian blue: methodology, possibilities and limitations. In: Doctoral Dissertation report. Institutionen för arkeologi och antikens kultur.
Stephens, M., Rose, J., Gilbertson, D.D., 2017. Post-depositional alteration of humid tropical cave sediments: micromorphological research in the great cave of Niah, Sarawak, Borneo. J. Archaeol. Sci. 77, 109–124.
Sugiyama, Y., Kurita, H., Matsui, T., Kimoto, S., Shimomura, T., 2009. Carrying of dead infants by Japanese macaque (*Macaca fuscata*) mothers. Anthropol. Sci. 117, 113–119.
Sunquist, M.E., Sunquist, F.C., 2009. Family Felidae (cats). Handbook of the Mammals of the World 1, 54–169.
Suraprasit, K., Jaeger, J.J., Chaimanee, Y., Chavasseau, O., Yamee, C., Tian, P., Panha, S., 2016. The middle Pleistocene vertebrate fauna from Khok Sung (Nakhon Ratchasima, Thailand): biochronological and paleobiogeographical implications. ZooKeys 613, 1–157.
Suraprasit, K., Jaeger, J.J., Chaimanee, Y., Sutcharit, C., 2020. Taxonomic reassessment of large mammals from the Pleistocene homo-bearing site of Tham wiman Nakin (northeast Thailand): relevance for faunal patterns in mainland Southeast Asia. Quat. Int.
Swindler, D.R., 2002. Primate Dentition: an Introduction to the Teeth of Non-human Primates. Cambridge University Press.
Swindler, D.R., Orlosky, F.J., 1974. Metric and morphological variability in the dentition of Colobine monkeys. J. Hum. Evol. 3, 135–160.
Teaford, M.F., 1982. Differences in molar wear gradient between juvenile macaques and langurs. Am. J. Phys. Anthropol. 57 (3), 323–330.
Thomas, D.H., 1971. On distinguishing natural from cultural bone in archaeological sites. Am. Antiq. 36, 366–371.
Tong, H., 2005. Dental characters of the Quaternary tapirs in China, their significance in classification and phylogenetic assessment. Geobios 38, 139–150.
Tong, H.W., Guérin, C., 2009. Early Pleistocene *Dicerorhinus sumatrensis* remains from the liucheng gigantopithecus cave, guangxi, China. Geobios 42, 525–539.
Tong, H.W., Liu, J.Y., Han, L.G., 2002. On fossil remains of early Pleistocene tapir (Perissodactyla, Mammalia) from fanchang, anhui. Chin. Sci. Bull. 47, 586–590.
Tougard, C., 1994. Etude d'une faune de grands mammifères (carnivores, ongulés et primates) du Pléistocène moyen de Thaïlande (Doctoral dissertation).
Tougard, C., 1998. Les faunes de grands mammifères du Pléistocène moyen terminal de Thaïlande dans leur cadre phylogénétique, paléoécologique et biochronologique. Ph. D. thesis, University of Montpellier II (unpubl.) Van Aarde, R.J., 1985. Age determination of Cape porcupines, Hystrix africaeaustralis. Afr. Zool. 20, 232–236.
Tougard, C., Chaimanee, Y., Suteethorn, V., Triamwichanon, S., Jaeger, J.J., 1996. Extension of the geographic distribution of the giant panda (Ailuropoda) and search for the reasons for its progressive disappearance in Southeast Asia during the Latest Middle Pleistocene. Comptes Rendus-Academie des Sciences Paris Serie 2 Sciences de la terre et des planets fascicule A 323, 973–979.
van den Bergh, G.D., de Vos, J., Sondaar, P.Y., 2001. The Late Quaternary palaeogeography of mammal evolution in the Indonesian Archipelago. Palaeogeogr. Palaeoclimatol. Palaeoecol. 171, 385–408.
Van Schaik, C.P., Van Noordwijk, M.A., 1985. Evolutionary effect of the absence of felids on the social organization of the macaques on the island of Simeulue (*Macaca fascicularis fusca*, Miller 1903). Folia Primatol. 44, 3–4.
Van Weers, D.J., 2005. A taxonomic revision of the Pleistocene *Hystrix* (Hystricidae, Rodentia) from Eurasia with notes on the evolution of the family. Contrib. Zool. 74, 301–312.
Villa, P., Mahieu, E., 1991. Breakage patterns of human long bones. J. Hum. Evol. 21, 27–48.
Wattanapituksakul, A., Filoux, A., Amphansri, A., Tumpeesuwan, S., 2018. Late Pleistocene caprinae assemblages of Tham lod rockshelter (mae hong son province, northwest Thailand). Quat. Int. 493, 212–226.
Westaway, K.E., Morwood, M.J., Roberts, R.G., Rokus, A.D., Zhao, J.X., Storm, P., Aziz, F., van den Bergh, G., Hadi, P., De Vos, J., 2007. Age and biostratigraphic significance of the Punung rainforest fauna, East Java, Indonesia, and implications for *Pongo* and *Homo*. J. Hum. Evol. 53, 709–717.
Westaway, K.E., Louys, J., Due Awe, R., Morwood, M.J., Price, G.J., Zhao, J.-x., Aubert, M., Joannes-Boyau, R., Smith, T., Skinner, M.M., Compton, T., Bailey, R.M., van den Bergh, G.D., de Vos, J., Pike, A.W.G., Stringer, C., Saptomo, E.W., Rizal, Y., Zaim, J., Santoso, W.D., Trihascaryo, A., Kinsley, L., Sulistyanto, B., 2017. An early modern human presence in Sumatra 73,000–63,000 years ago. Nature 548, 322–325.
Willis, M.S., Swindler, D.R., 2004. Molar size and shape variations among Asian colobines. Am. J. Phys. Anthropol. 125 (1), 51–60.
Wolff, R.G., 1973. Hydrodynamic sorting and ecology of a Pleistocene mammalian assemblage from California (USA). Palaeogeogr. Palaeoclimatol. Palaeoecol. 13 (2), 91–101.
Woodruff, D.S., 2010. Biogeography and conservation in Southeast Asia: how 2.7 million years of repeated environmental fluctuations affect today's patterns and the future of the remaining refugial-phase biodiversity. Biodivers. Conserv. 19, 919–941.
Yan, Y., Wang, Y., Jin, C., Mead, J.I., 2014. New remains of rhinoceros (Rhinocerotidae, Perissodactyla) associated with gigantopithecus blacki from the early Pleistocene yanliang cave, fusui, South China. Quat. Int. 354, 110–121.
Zeitoun, V., Chinnawut, W., Arnaud, L., Bochaton, C., Burdette, K., Thompson, J., Mallye, J.B., Frère, S., Debruyne, R., Antoine, P.O., William, J.R., 2019. Dating, stratigraphy and taphonomy of the Pleistocene site of ban fa suai II (northern Thailand): contributions to the study of paleobiodiversity in Southeast Asia. In: Annales de Paléontologie, vol. 105, pp. 275–285.

Zhang, S., Li, Z., Zhang, Y., Gao, X., 2009. Mortality profiles of the large herbivores from the lingjing xuchang man site, henan province and the early emergence of the modern human behaviors in east Asia. Chin. Sci. Bull. 54, 3857–3863.
Zhang, H., Wang, Y., Janis, C.M., Goodall, R.H., Purnell, M.A., 2017. An examination of feeding ecology in Pleistocene proboscideans from southern China (*Sinomastodon, Stegodon, Elephas*), by means of dental microwear texture analysis. Quat. Int. 445, 60–70.
Zhang, B., Chen, X., Tong, H.W., 2018. Tooth remains of late Pleistocene moschid and cervid (Artiodactyla, Mammalia) from yangjiawan and fuyan caves of southern China. Quat. Int. 490.